ACS OMEGA

Open Access

http://pubs.acs.org/journal/acsodf

Article

8-Aminoquinoline-Based Promising Zn Complexes with Dicyanamide and Tricyanomethane Anions: Supramolecular $R_4^4(8)$/$R_2^2(16)$ Synthons, DFT Rationalization, and Biological Insights

Suman Hazra, Dhrubajyoti Majumdar,* Jessica Elizabeth Philip, Bouzid Gassoumi, Antonio Frontera, Sourav Roy, Houcine Ghalla, and Sudipta Dalai*

Cite This: *ACS Omega* 2025, 10, 14770−14786

Read Online

ACCESS | Metrics & More | Article Recommendations | Supporting Information

ABSTRACT: Considering the new crystal engineering integrity utilizing the DFT and the issues surrounding antimicrobial resistance in complexes, there is a pressing need to tackle antifungal photodynamic therapy about global health challenges. Within the sphere of this study, we meticulously introduce the synthesis, characterization, and single-crystal structure of two 8-aminoquinoline-based Zn complexes $[Zn\{(8\text{-AMQ})\ (X)\}_2]$, X = dca (**1**) and TCM (**2**). The X-ray study reveals that the complexes crystallize in the monoclinic and triclinic space groups $P2_1/c$ and $P\text{-}1$. The crystal packing in both complexes feature N−H···N hydrogen bonds as well as weak C−H···N interactions. The Hirshfeld surface provides quantitative insight into various supramolecular interactions, including $\pi\cdots\pi$ stacking, at large Cg···Cg distances. FMO supports the complexes' conductive behavior, excellent stability, and reactivity parameters. DOS investigation suggests good conductivity and reactivity properties. NBO analyzed that **2** exhibits a greater reactive and high potential charge transfer mechanism. The QTAIM/NCI-RDG plot ensured N···Zn/H···N interactions and explored new supramolecular R_4^4 (8)/$R_2^2(16)$ crystal engineering synthons. The Trypan blue exclusion method was used to evaluate cytotoxicity against the DLA cell line, demonstrating **1**'s effectiveness against the cell, the lowest % of cell death, and a promising anticancer agent. The Zn complex antifungal photodynamic therapy finding showed significant activity against *C. albicans*.

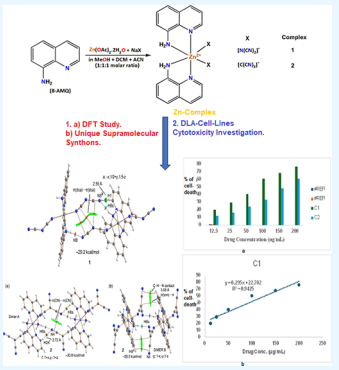

INTRODUCTION

N-rich 8-aminoquinoline (8-AMQ) and its metal complexes have recently gained attention for their medicinal antiprotozoal properties[1] and diverse boundless applications in coordination chemistry.[2] Thus, exploring the flexibility of 8-AMQ organic ligand (L^{ORG}) in biological and supramolecular chemistry is limitless.[1,2] The 8-AMQ-uracil metal complexes have shown promising biological properties (anticancer and antimalarial activity, superoxide scavenging, and antimicrobial activities),[1,3] offering hope for new potential applications. 8-AMQ possesses a significant chelating planar arrangement and showcases exceptional properties, making it a fascinating attraction in supramolecular chemistry.[2,4] The ligand NH_2 functional group's ability to bind with M^{n+} (metal) ions and form H-bonding and its potential for impressive engagement in $\pi-\pi$ stacking interactions with aromatic C_6H_6 moiety and regulate interlocking network interpenetration (Scheme S1).[2,4] Interpreting the "supramolecular" term is strongly linked to manipulating self-assemblies via interactions between M (metal) and L^{ORG} and various intermolecular forces.[5] The crucial factors for controlling self-assembly under crystal engineering include the M-center, used co-ions (X) nature (X = dca/TCM), L^{ORG} steric and conformational properties, and the reaction medium.[2,6] Generally, supramolecular networks in polymers can be developed by utilizing CB (coordination bonds), H-bonds, and aromatic $\pi-\pi$ stacking interactions.[2] Recently, synthetic chemists have been using dicyanamide (dca) and tricyanomethane (TCM) coligands to broaden the scope of supramolecular chemistry and crystal engineering in their synthesized metal complexes.[7] Notably, the exploration of $[C(CN)_3]^-$ and $[N(CN)_2]^-$ as ligands in coordination chemistry started just three decades ago.[8] These ions are utilized as building blocks due to their versatile binding propensity with M^{n+} ions (Scheme S2−S3), which enhance the flexibility of creating discrete molecules or polymeric networks.[7] Scientist Madelung published the first report on DCA involving coordination compounds. In 1922, Kern discovered its ability to coordinate with 3d transition M^{n+} ions, which Kohler et al. further investigated in the 1960s and 1980s.[8] Therefore, extensive research has been conducted using transition metal based on DCA/TCM anions (Scheme S1).[7] This research has examined novel crystal structures and

Received: October 11, 2024
Revised: March 27, 2025
Accepted: March 31, 2025
Published: April 7, 2025

their properties concerning supramolecular chemistry and new bonding concepts (Spodium/σ/π-hole).[9] Therefore, extensive studies on d^{10} metal complexes provide a solid foundation for further research.[10] Again, Zn metal is well-known in biology, and some of its complexes can mimic the active sites of zinc metalloenzymes.[11] The d^{10} electronic configuration of Zn(II) allows for different coordination geometries in its complexes.[12,7d] These are all intriguing sights for synthetic chemists pursuing Zn(II) metal ion research. Furthermore, FMO/ESP/NBO/QTAIM/NCI-RDG/ELF-LOL studies are gaining popularity and becoming common in exploring the unique properties of synthesized complexes.[13,14] This trend is not temporary but is rising.[15] Meanwhile, cancer research and antifungal photodynamic therapy (APDT) have gained popularity among new-generation scientists. Extensive research has already focused on nonplatinum-based metal-chemotherapeutic drugs for treating a more comprehensive range of cancers with reduced toxicity.[16] DLA cells play a crucial role in this research. Various Zn complexes have been tested for their cytotoxicity against DLA cells.[16] Further, antimicrobial resistance research is a significant global health concern. *C. albicans* is a common cause of invasive fungal infections. APDT is an alternative treatment that can eliminate microorganisms.[17]

Considering the precedence significance of the 8-AMQ ligand and its complexes, we synthesize, and X-ray characterize two Zn complexes. DFT study investigates the Zn complex's reactivity and supramolecular and hydrogen bonding (N···H/H···N) perspectives. The QTAIM/NCI-RDG explores supramolecular $R_4^4(8)/R_2^2(16)$ synthons under crystal engineering. The cytotoxicity of the complex and its antifungal photodynamic therapy were analyzed in detail.

EXPERIMENTAL SECTION

Materials. Reagent-grade chemicals and solvents were used without additional purification. $Zn(OAc)_2.2H_20$, 8-aminoquinoline (8-AMQ), Sodium dicyanamide (Nadca), and Sodium tricyanomethane (TCM) were directly purchased from Sigma-Aldrich USA Company. The solvents CH_3OH, Dichloromethane (DCM), and Acetonitrile (ACN) were obtained from SRL (Sisco Research Laboratories) Pvt. Ltd. India.

Physical Measurements. The elemental composition (CHN) was analyzed using a PerkinElmer 2400 CHN elemental instrument, while high-resolution mass spectrometry (HRMS) was conducted using a Xevo G2-XS QToF 4k instrumental model with an H-Class PLUS UPLC system. IR/Raman spectra were examined using PerkinElmer and Bruker RFS 27 instruments. NMR spectra were analyzed in DMSO-d6 solvents with a Bruker FT-NMR spectrometer. The Oxford XMX N model was used for EDX analysis, and SEM images were taken with a JEOL JSM-6390LV. UV−vis measurements were conducted using a Hitachi U-3501, and powder X-ray diffraction was performed with a BRUKER AXS model. The Thermo-Scientific NEXA analyzer was utilized for XPS spectra analysis.

Synthetic Methodology. *[Zn{(8-AMQ) (dca)}$_2$] (1).* In a 100 mL round-bottom flask, 0.219 g of Zn(II) acetate dihydrate (1 mmol) and 0.144 g of 8-aminoquinoline (1 mmol) were dissolved in a mixture of 15 mL CH_3OH, DCM, and ACN solvents (1:1:1 molar ratio) after stirring for 30 min at a constant temperature of 65 °C on a magnetic stirrer. Then, a 5 mL methanol solution of Nadca was dropwise added and mixed after shaking in a mechanical shaker for 3 min. The solution was stirred using a magnetic stirrer for 30 min. The colorless solution was cooled, filtered, and then evaporated slowly for crystallization at room temperature. The plate-shaped single crystals suitable for SCXRD were collected and air-dried. Yield: (62%), Anal. Calc. for $C_{22}H_{16}N_{10}Zn$: C, 54.39; H, 3.32; N, 28.83, Found: C, 54.43; H, 3.29; N, 28.88, HRMS for complex, (m/z, TOF MS): found for 485.09 (calculated 485.82), IR (KBr cm^{-1}) selected bands: for ν(Nadca), 2180−2362, and for 8-AMQ, ν(N−H), 3355−3450, ν(C=C), 1615, ν(phenyl ring), 1428, 1364, for complex **1**, ν(N−H), 3160, ν(C=C), 1600, ν(phenyl ring), 1410, 1340, ν(Zn−N), 585, ν(C−N−Zn), 1039, 1206, ν(dca), 2188, FT-Raman (cm^{-1}) selected bands: ν(C=C), 1603 s, ν(phenyl ring), 1448, 1365 s, ν(Zn−N), 584 m, ν(C−N−Zn), 1042, 1200 m, ν(dca), 2188−2238 s, ^{1}H NMR (DMSO-d_6, 400 MHz): δ (ppm): for 8-AMQ, 6.92−7.36 (Ar CH), 7.37 (NH_2 proton), 8.76−8.77 (Ar CH), ^{13}C NMR (DMSO-d_6, 75.45 MHz): δ (ppm): For 8-AMQ, 110.15−128.93 (C Ar), 136.09−147.53 (C Ar), ^{1}H NMR (DMSO-d_6, 400 MHz): δ (ppm): for complex **1**, 6.84−7.42 (Ar CH), 7.43 (NH_2 proton), 8.14−8.69 (Ar CH),), and ^{13}C NMR (DMSO-d_6, 75.45 MHz): δ (ppm): 109.08−128.57 (C Ar), 135.94−147.04 (C Ar), UV−vis λ_{max} (DMF): 258 and 375 nm.

[Zn{(8-AMQ) (TCM)}$_2$] (2). We employ a comparable method for synthesizing complex **2**, using a 5 mL methanol solution of TCM instead of Nadca. Yield: (63%), Anal. Calc. for $C_{26}H_{16}N_{10}Zn$: C, 58.49; H, 3.02; N, 26.24, Found: C, 58.52; H, 3.0; N, 26.22, HRMS for complex, (m/z, TOF MS): found for 533.08 (calculated 533.88), IR (KBr cm^{-1}) selected bands: for ν(TCM), 2178, and for complex **2**, ν(C=C), 1607, ν(phenyl ring), 1370, 1422, ν(Zn−N), 582, ν(C−N−Zn), 1075, 1242 m, ν(TCM), 2175, FT-Raman (cm^{-1}) selected bands: ν(C=C), 1600 s, ν(phenyl ring), 1439, 1390 s, ν(Zn−N), 582 m, ν(C−N−Zn), 1082, 1238 m, ν(TCM), 2170−2220 s, ^{1}H NMR (DMSO-d_6, 400 MHz): δ (ppm): for complex **2**, 6.84−7.42 (Ar CH), 7.43 (NH_2 proton), 8.14−8.69 (Ar CH),), and ^{13}C NMR (DMSO-d_6, 75.45 MHz): δ (ppm): 109.84−128.64 (C Ar), 136.12−147.18 (C Ar), UV−vis λ_{max} (DMF): 345, 265, and 220 nm.

X-ray Crystallography. Table 1 provides detailed crystallographic data and information about refining the Zn complex structures. The complexes in good-quality crystal form were grown by slowly evaporating them at room temperature from a solvent medium of CH_3OH+DCM +ACN. The crystals of the two Zn compounds were examined using a Bruker-AXS SMART APEX II diffractometer.[18] with standard Mo Kα radiation. Two Zn complex structures were solved using various crystal-solving programs. SMART[18] employs different approaches to collect vital crystallographic data. The software detects frames that contain data, assesses the reflections, and computes the lattice parameters. SAINT[18] enhances the reflection combination, while SADABS[18] corrects the absorption. SHELXTL and least-squares methods accurately determined the space group (SG), structure, and F^2. Complex crystal structures were examined using full-matrix least-squares methods and refined using SHELXL-2014[18] and Olex-2 software.[18] The crystal was refined by applying anisotropic shift parameters to all atoms. The hydrogen atoms are refined isotropically. Diamond's software generated various molecular diagrams with crystallographic structures.

Quantum Chemical Methods. The Zn complexes has been optimized using DFT/B3LYP-D3/Lanl2DZ,[19] imple-

https://doi.org/10.1021/acsomega.4c09312
ACS Omega 2025, 10, 14770−14786

Table 1. Crystal Data and Structure Refinement for the Zn Complexes

empirical formula	$C_{22}H_{16}N_{10}Zn$ (**1**)	$C_{26}H_{16}N_{10}Zn$ (**2**)
formula weight	485.82	533.86
temperature/K	296.15	296.15
crystal system	monoclinic	triclinic
space group	$P2_1/c$	P-1
a/Å	8.9494(19)	7.977(2)
b/Å	7.4425(16)	8.531(3)
c/Å	17.583(4)	10.000(3)
α/°	90	72.486(7)
β/°	115.609(6)	67.845(7)
γ/°	90	85.991(8)
volume/Å^3	1056.1(4)	600.4(3)
Z	2	1
ρ_{calc}g/cm^3	1.528	1.477
μ/mm^{-1}	1.197	1.060
F(000)	496.0	272.0
crystal size/mm^3	0.1 × 0.06 × 0.02	0.15 × 0.06 × 0.02
radiation	MoKα (λ = 0.71073)	MoKα (λ = 0.71073)
2Θ range for data collection/°	5.048 to 50.058	4.606 to 50.918
index ranges	$-10 \le h \le 10$, $-8 \le k \le 8$, $-20 \le l \le 20$	$-9 \le h \le 9$, $-10 \le k \le 10$, $-12 \le l \le 12$
reflections collected	32,701	19,988
independent reflections	1865 [R_{int} = 0.1071, R_{sigma} = 0.0395]	2218 [R_{int} = 0.0814, R_{sigma} = 0.0444]
data/restraints/parameters	1865/0/152	2218/0/170
goodness-of-fit on F^2	1.024	1.049
final R indexes [$I \ge 2\sigma$ (I)]	R_1 = 0.0425, wR_2 = 0.1016	R_1 = 0.0364, wR_2 = 0.0699
final R indexes [all data]	R_1 = 0.0696, wR_2 = 0.1173	R_1 = 0.0548, wR_2 = 0.0771
largest diff. peak/hole/e Å^{-3}	0.44/−0.38	0.21/−0.31

mented in Gaussian09 software.[20] The graphs were generated using the Gauss View 6 package.[21] The FMO, MEP figures were computed using the TD-DFT/B3LYP-D3 method.[22,23,7b] The geometries of the Zn complexes were calculated using crystallographic coordinates and based on the theory PBE0-D3/def2-TZVP[24] in the Gaussian-16 program.[25] The electron density has been analyzed using the "atoms-in-molecules" (AIM)[26] and NCI plot[27] analyses using the AIM All program. The LED (Laplacian of electron density) can be broken down into contributions along the three principal axes of maximum variation.[28] The 3D-Hirshfeld Surface/2D fingerprint plot details were presented in ESI.

Biological Studies. *Drug Preparation and % of Cytotoxicity Determination.* The synthesized compounds were tested for *in vitro* cytotoxicity using the TBEM (Trypan Blue Exclusion Method) at various concentrations. The cytotoxicity of the test compound was evaluated based on DLA (Dalton's Lymphoma Ascites) cells. Cells are cleaned three times using PBS (phosphate-buffered saline) or a standard cell line. The TBEM was utilized to evaluate cell viability according to standard experimental procedures. The tested sample was analyzed in triplicate.[29] Data were presented as the mean ± standard deviation (SD). SPSS Base 16 (SPSS Inc., Chicago, IL) and ANOVA were utilized for statistical analysis.

$$\%\text{Cytotoxicity} = \frac{\text{No. of dead cells}}{\text{No. of live cells} + \text{No. of dead cells}} \times 100$$

APDT and MIC Determination. C. albicans (ATCC 10231) was sourced from the American Type Culture Collection (ATCC, Manassas, VA, USA), and the media was purchased from Himedia, India. The antifungal activity of the synthesized compounds against *C. albicans* was evaluated using the WDM (Well Diffusion Method). APDT studies were conducted on **1** and **2**. The testing samples underwent irradiation for 2 h utilizing a 300 W Newport Xenon arc lamp (designed irradiated samples are C**1*** and C**2***) (where antibiotic griseofulvin, and DMSO was utilized as a negative control). The study used the well-known MBDM (Micro Broth Dilution Method) to establish the irradiated samples MIC. The fluoroprobe PBA did not show activity against the two strains in this research.[30]

RESULTS AND DISCUSSION

Two water-insoluble centrosymmetric mononuclear Zn complexes [Zn{(8-AMQ) (X)}$_2$], (X = dca/TCM) with dca (**1**) and TCM (**2**) ions were synthesized via self-assembly *in situ* technique (Scheme 1). Several physicochemical methods, including XPS techniques, structurally characterize the compounds. The Zn complexes with 8-AMQ ligands exhibit restricted coordination chemistry concerning X-ray crystal structures, especially in the presence of X ions (Scheme S1).[2,4,7,8] However, the literature has no information for Zn-8 AMQ complexes with X anions concerning DFT investigations, APDT, and cytotoxicity against DLA cell lines. Notably, the first time we are exploring N···Zn/H···N and weak C−H···N supramolecular interactions using QTAIM/NCI-RDG plot, crystal engineering R_4^4 (8)/R_2^2(16) synthons.

Scheme 1. Synthetic Outline for the Zn Complexes

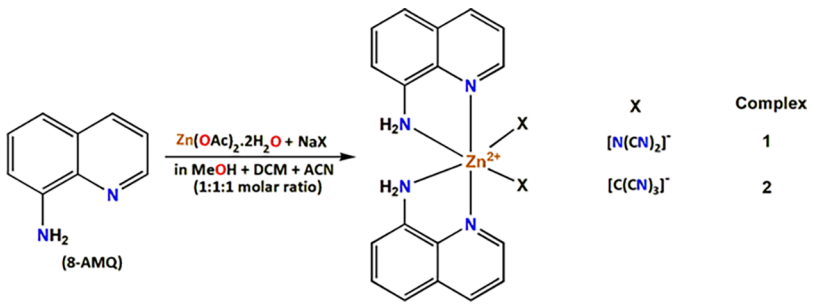

https://doi.org/10.1021/acsomega.4c09312
ACS Omega 2025, 10, 14770−14786

Structural Characterization. *HRMS Analysis.* The two zinc complexes feature an 8-AMQ structural frame connected by dca and TCM ions. The complexes were characterized using high-resolution mass spectroscopy (HRMS) (Figures S1−S2). The molecular ion peaks for the Zn complexes were observed at 485.09 m/z (calculated 485.82, **1**) and 533.08 m/z (calculated 533.88, **2**), confirming the Zn metal complexes' stoichiometry.

IR and Raman Spectroscopy. We characterize the Zn complexes using IR and Raman spectroscopic studies (Figures S3a-c, S4a-b, and S5). The IR/Raman spectral analysis of **1** and **2** depends entirely on the stretching values of ν(N−H), ν(C=C), ν(phenyl ring), ν(Zn−N), and ν(C−N−Zn). Moreover, spacers like dca and TCM anions are joined in Zn complexes. Henceforth, IR/Raman characterization relies also on the stretching band identification of ν(dca) and ν(TCM). Before completing Zn complex structural characterization, we first need to analyze the ligands of 8-AMQ thoroughly. In 8-AMQ, stretching values of ν(N−H), ν(C=C), ν (phenyl ring) are observed at 3355−3450, 1615, 1428, 1364 cm^{-1}, respectively. In the case of **1** & **2**, these stretching shifted values are observed at 3160, 1600, 1410, and 1340 cm^{-1} (**1**) and 3165, 1607, 1370, 1422 cm^{-1} (**2**), respectively.[7,8] Further, in both complexes, ν(Zn−N) and ν(C−N−Zn) values are observed at 585, 1039, 1206 cm^{-1} (**1**) and 582, 1075, 1242 cm^{-1} (**2**).[7,8] All these shifting IR stretching values confirm that in both Zn complexes, AMQ is present, and 8-AMQ N-donor centers are coordinated to Zn ions to form bonds Zn−N and C−N−Zn. The most exciting identification for the Zn complexes is the presence of dca and TCM. The Zn complexes' shifting peaks near 2188, and 2175 cm^{-1} confirm that the dca and TCM anions are linked to the zinc metal centers.[7b,c,8]

UV−Vis Spectrum. The UV spectra of Zn complexes were examined in DMF solvent (Figure S6). The UV spectrum of the complex's broad peaks is observed at 258 and 375 nm (**1**) and 345, 265, and 220 nm (**2**). The results indicate that the 8-AMQ interacts with Zn^{2+} through N-donating atoms, which can be ascribed to a transition involving the $\pi \rightarrow \pi^*$ aromatic benzene ring.[7b,c] The optical transition of the Zn complex is distinct from that of the Quinoline ligand because of a reduced energy of the HOMO−LUMO resulting from π overlapping of the ligands in the complex. The Zn^{2+} possesses a $3d^{10}$ arrangement, and the HOMO−LUMO orbitals of the complexes are spread out across the quinoline moiety. The characteristic of the HOMO and LUMO orbitals of the separate quinoline unit stays unchanged under the condition. This electronic transition type resembles the other Zn complexes.[31] The peak absorption of the Zn complexes moved to a longer wavelength (nm), indicating the charge transfer from the Zn→8-AMQ (M→LCT bands).[31]

^{1}H and ^{13}C NMR. We characterize the Zn complexes using an NMR spectral investigation (Figures S7a-b, S8a-b, and S9a-b). Therefore, the NMR analysis of **1** and **2** depends entirely on the aromatic carbon ring frame with the N-donor ligands 8-AMQ. Hence, the structural arrangements of 8-AMQ and the Zn compounds were examined based on NMR. We first did an NMR investigation for the 8-AMQ to establish the Zn complex's structural framework. For the 8-AMQ, ^{1}H NMR peaks are observed at δ (ppm): 6.92−7.36 and 8.76−8.77 ppm, responsible for the Ar CH proton nature.[7b,c] A peak at δ 7.37 is identified for the NH_2 proton. Similarly, the ^{13}C NMR study identified peaks as δ 110.15−128.93 ppm and δ 136.09−147.53 ppm, corresponding to the aromatic carbon. Based on 8-AMQ NMR studies, a noticeable shifting of NMR peaks is observed for the Zn complexes. For **1**, Ar CH proton shifting nature δ 6.84−7.42 ppm and δ 8.14−8.69 ppm. Also, the NH_2 proton shifting is δ 7.43 ppm. In contrast, for **2**, Ar CH and NH_2 proton shifting nature δ 6.84−7.42 ppm and δ 8.14−8.69 and 7.43 ppm, respectively.[7b,c] These ^{1}H NMR peak values confirmed that Zn complexes have an aromatic carbon ring and are coordinated with 8-AMQ N-donor centers. The shifting of ^{13}C NMR peak values further substantiates both complexes' aromatic carbon structural frames (see shifting peak values δ: 109.84−128.64 ppm and 136.12−147.18 ppm).

EDX-SEM Approach. The scanning electron microscope (SEM) is widely used to analyze the structural morphology and size of Zn complexes.[32] Energy-dispersive X-ray (EDX) analysis involves using X-rays to establish the chemical composition of a synthesized material. The Zn complexes EDX spectrum (Figure S10a-b) defines the elemental and metal composition. According to the EDX profiles, it is concluded that **1** is composed of carbon (C), nitrogen (N), oxygen (O), and Na/Zn metal ions. Similarly, **2** comprises carbon (C), nitrogen (N), and Zn metal ions. The EDX information also suggests their weight percentage (Table S1). Moreover, the EDX profile confirms the interaction between Zn^{2+} ions and the N-donor 8-AMQ in the presence of dca and TCM anions. Upon examination of SEM micrographs (Figures S11a-e and S12a-e), it was found that the surface structure of the Zn complexes resembled an organized ice type. For **1**, SEM graphs (a-e) divulge the ice-type morphology. Up to 10−50 μm, the ice morphology surface is rough, gradually developing more organized ice at 1 μm. The same concept applies to **2** SEM graphs (a-e). A literature study explored dramatic particle size and morphology differences from other quinoline-based metallic complexes.[31a] Zn complexes were found to possess more consistent size and ice morphology characteristics, possibly due to the more substantial effect of 8-AMQ conjugation on the Zn^{2+} ion.

Powder X-ray Diffraction. The Zn complexes were analyzed using powder X-ray diffraction to determine their crystallinity by examining the X-ray powder diffraction patterns. The PXRD investigated that the Zn complexes coordinated through the N-donor atom of the 8-AMQ (Figure S13a-b) are pure in phase and have an excellent crystalline nature. The solid Zn crystals exhibited a PXRD pattern that closely resembled the simulated XRD pattern before and after deposition, indicating a successful experimental match. The results from the PXRD analysis show their concurrence. The CCDC Mercury software created the simulated pattern utilizing the single-crystal X-ray diffraction data in CIF format for the Zn complexes. The sharp diffraction peaks suggest that the synthesized Zn crystal products have high crystallinity. Further, PXRD analysis concluded that the bulk material comprises a single crystal.

X-ray Photoelectron Spectroscopy. X-ray photoelectron spectroscopy (XPS) is used to analyze the elemental composition and support the formation of two zinc complexes with 8-AMQ ligands in the presence of dca (**1**) and TCM (**2**) ions (Figure S13c-d/Table S2).[7b] The successful scanning of the XPS spectrum confirms the presence of O, N, C, and Zn metal ions in the 8-AMQ complexes.[33] Concerning the X-ray crystal structure of complexes, it is clear that the Zn(II) ion is linked with the N-donor 8-AMQ along with N-bonded dca (**1**) and TCM (**2**) ions. Therefore, Zn was identified using a Zn 2p, Zn 3p, and Zn 3d XPS scan image (BE 1022,1045, 89.3, 89.2

https://doi.org/10.1021/acsomega.4c09312
ACS Omega 2025, 10, 14770−14786

and 11.0, 10.8 eV). The above statement further confirmed that the Zn atoms in both complexes are entirely in the Zn^{2+} form.[33] The Zn complexes XPS scan obtained binding energy corresponding to the peaks C 1s, N 1s, and O 1s are 285, 399.5, and 531 for **1**, while for **2**, 285, 399.2, and 531 eV, respectively.[33] The 285 eV C 1s XPS spectrum peak in both Zn complexes can be assigned to the C atoms present in the C−C bond framework.[33] Similarly, the N 1s XPS spectrum's two peaks, at 399.5 for **1** and **2** 399.2 eV, are associated with the electron-rich nitrile nitrogen in the dca and TCM ions present in the complex structures.[33] Therefore, the N 1s XPS scan identifies the formation of the dca (**1**) and TCM (**2**) complexes based on their respective binding energies (eV).

X-ray Crystal Structure Description. The X-ray single-crystal structure determination reveals that **1** crystallizes in monoclinic space group $P2_1/c$, while **2** crystallizes in triclinic space group $P\text{-}1$. The two Zn complexes are centrosymmetric and built from the isolated mononuclear moiety of [Zn{(8-AMQ) (X)}$_2$] where X is dicyanamide (dca) in **1**, and tricyanomethane (TCM) in **2**. Table 2 show the Zn complex's

Table 2. Selected Bond Lengths (Å) and Angles (°) in the Zn Complexes

Bond lengths for Zn complexes **1** and **2**			
atom	atom	length/Å (**1**)	length/Å (**2**)
Zn1	N1	2.113(3)	2.126(3)
Zn1	N2	2.162(4)	2.104(2)
Zn1	N3	2.206(3)	2.298(3)
Bond angles for Zn complexes **1** and **2**			
atom	atom	atom	angle/°(**1**)	angle/°(**2**)
N1	Zn1	N3	89.43(15)	86.35(9)
N2	Zn1	N1	78.85(13)	79.86(9)
N2	Zn1	N3	86.46(13)	88.19(10)

significant crystallographic parameters. Figure 1 (top) presents perspective views of both complexes, while Figure 1 (bottom) represents the polymeric network of complexes. The asymmetric unit contains one ligand (8-AMQ), one metal center, Zn(II), and one coligand [(dca) in **1**, and (TCM) in **2**] for both complexes. The metal center, Zn (1), is hexacoordinated where the amine nitrogen's [N (2), N(2)^a] and pyridine [N (1), N(1)^a] {^{a}=-X,-Y,1-Z} nitrogen's from two amino-quinoline (AMQ) forming the basal plane in both complexes. Two nitrogen atoms, [N (3), N(3)^b] from two dicyanamide ligands in **1** and two TCM in **2** coordinated with the Zn metal centers from the axial sites, completing its coordination number and resulting in slightly distorted octahedron geometries. The Zn−N bond lengths are comparatively longer in {2.206 (3) Å in **1** and 2.298 (3) Å in **2**} than in the basal site {2.137 (3) Å in **1** and 2.115 (3) Å in **2**}.

Supramolecular Interactions. Crystal packing in both Zn complexes consist of N−H···N hydrogen bond interactions. Weak C−H···N interactions are also noticed in **1**. In both complexes, the amine hydrogen atoms, H2A and H2B, attached to the nitrogen atom, N (2), form intermolecular hydrogen bonds with symmetry-related nitrogen atoms from dca in **1** and TCM in **2**. In **1**, these hydrogen bonds form a tetramer (Figure 2). Hydrogen atom, H (1), attached to the carbon atom, C (1), also participates in a C−H···N interaction with a nitrogen atom, N (5) from a dca coligand in complex **1** (Figure 2, top). In **2**, the N−H···N interactions form a hexamer like structure (Figure 2, bottom). The details of the geometric features for both complexes are presented in Tables 3-4. Both complexes exhibit $\pi\cdots\pi$ interactions between the planar 8-AMQ ligands. The 10-membered ring, Cg (5), of both complexes is involved in intermolecular $\pi\cdots\pi$ interaction with symmetry-related Cg (5) rings from nearby molecules to form a 1D structure as shown in Figures 3 (top-bottom).[33] The details of the geometric features are given in Table 5.

DFT Investigations. *Hirshfeld Surface and 2-D Fingerprint Plots.* The Zn complexes 3D-HS and 2D-fingerprint plots are illustrated in Figures S14−15, and the Hirshfeld surface's significant findings are submitted in Section S1.

FMO and Global Reactivity Parameters. The energy difference between the HOMO and LUMO delineated the gap energy, which serves as an indicator of the chemical and kinetic stability of the complex.[34] This parameter gives valuable insights into the conductivity properties and reactivity of the system. Herein, we concentrate FMO analysis on two complexes (**1**−**2**) (Figure 4). It was observed that the HOMO orbital enveloped the Zn of two ligands. Afterward, these electrons pass through the energy barrier, which is not allowed, with energies of around 3.21 and 2.73 eV. They move to the N-ring ligand (LUMO band). This finding elucidates the presence of significant electron concentrations surrounding the central metal zinc (Zn), indicating a considerable electron charge transfer phenomenon between ligands interacting with Zn. This result indicates the importance and suitability of our materials for enhancing electronic devices, as compared to the reported literature.[34d−f] Furthermore, a noteworthy outcome is the formation of donor and acceptor ligands with the same molecular framework, highlighting their potential applicability in nanoelectronic devices. Also, it was found that **2** had more conductive behavior, more excellent stability, and higher reactivity than **1**. The different quantum chemical parameters are computed based on Koopman's theorem (Table 6).

DOS Profile: True Concept of Electronic Modules. The DOS spectra of the two Zn complexes are depicted in Figure 5. DOS graphs indicate that the HOMO and LUMO values demonstrate the chemical stability of the two complexes. Furthermore, these values elucidate the charge transfer mechanism and exhibit high polarizability. The low values of hardness η (1.50 and 1.36 eV) and the large electronegativity value χ (4.35 and 4.36 eV) indicate a facile transition of electrons from fundamental state to excited state, facilitating the effective formation of electronic charge transfer with the guest. These findings suggest our new synthesis system's potential application in newly developed electronic modules. Also, this phenomenon is further corroborated by the HOMO/LUMO analysis. The significant value of ω (17.55 eV) suggests good reactivity properties of the two Zn complexes.

MEP Analysis. The MEP surface is essential for elucidating Zn compounds' chemical stability and reactivity and investigating the nucleophilic and electrophilic sites within the studied molecules.[35] MEP is a crucial technique for highlighting the donor and acceptor groups that enhance the stability of complexes, thereby clarifying the suitable applications of the system under investigation. Distinct color codes denote the donor and acceptor regions. Red represents the electrophilic acceptor regions (AR), while blue signifies the nucleophilic donor region (DR). The MEP iso-surfaces of the two complexes have been illustrated in Figure 6 (LHS for **1**, and RHS for **2**). It is observed that the acceptor regions

https://doi.org/10.1021/acsomega.4c09312
ACS Omega 2025, 10, 14770−14786

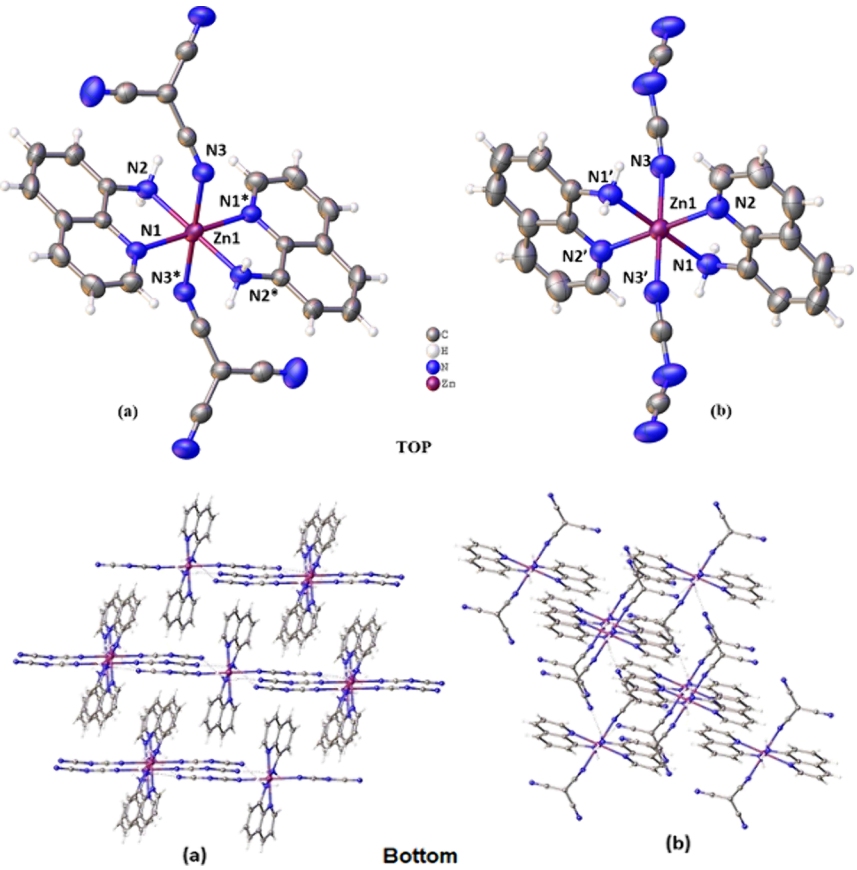

Figure 1. a-b. Perspective view of complex 1a and 2b (top) with selective atom numbering scheme. [Symmetry elements:' = -x,1-y,1-z; * = -x, -y,1-z] (ORTEP ellipsoid probability 50%). The dashed line represents the symmetry-related part of the complex; and Polymeric network of both complexes (bottom) [Ball and stick model].

(nucleophilic attack) are located around the Zn−C ligands. In contrast, the donor regions (electrophilic attack) are positioned to envelop the two N-ring ligands. This result suggests a significant charge transfer mechanism is taking place on the surface of the two complexes, a finding that is further corroborated by FMO analysis. Moreover, acceptor and donor regions within the same system are particularly advantageous for conductive and electronic transport materials. This discovery positions our novel synthesis system as a promising nanoelectronic application model. Additionally, the MEP is positive at the aromatic hydrogen atoms and over the π-system of the coordinated 8-aminoquinoline ring, with values ranging from 15.1 to 20.1 kcal/mol, being more positive over the pyridine ring. This MEP analysis confirms the strong propensity of the Zn-coordinated amino groups to act as hydrogen bond donors and the anionic coligands (dca/TCM), via their sp-hybridized N atoms, to serve as hydrogen bond acceptors (Figure S16).

NBO Analysis. Section S2 submitted the details fundamental principle of NBO. The Zn complexes NBO results from the second-order perturbation theory analysis of the Fock Matrix on a natural bond orbital (NBO) basis are presented in Table S3−S4 (kcal/mol). The atomic labels for both **1** and **2** are shown in Figure S17. The NBO analysis for **1** reveals significant hyper-conjugative interactions, detailed as follows: LP (2) N9 → BD* (3) (N6 - C8) (98.72 kcal/mol), LP (2) N9→ BD* (3) (N11 - C12) (56.70 kcal/mol), LP (2) N33→ BD* (3) (N30 - C32) (98.75 kcal/mol), and LP (2) N33→ BD* (3) (N35 - C36) (56.70 kcal/mol). In NBO analysis of **2**, LP (1) C9→ π* (N6 - C11) (105.57 kcal/mol), LP (1) C9→ π* (N12 - C13) (61.58 kcal/mol), LP (1) C9→ π* (N20 - C21) (58.91 kcal/mol), LP (1) C35→ π* (N32 - C37) (105.58 kcal/mol), LP (1) C35→ π* (N38 - C39) (61.59 kcal/mol), and LP (1) C35→ π* (N46 - C47) (58.91 kcal/mol) interactions showed that the carbon lone pair orbitals contribute to strong resonance interactions with the adjacent π* (C≡N) antibonding orbitals. The same interactions for nitrogen-rich compounds were also previously documented in the literature.[35c] These findings concluded the well-organized structure and stability of the two novel synthesis complexes, attributed to hyper-conjugative and nonbonding interactions. Furthermore, they demonstrate that **2** exhibits greater reactive and high potential charge transfer mechanism compared to **1.**

QTAIM/NCI-RDG Plots. Exploration of N···Zn/H···N Interactions. Section S3 submitted the details fundamental principle of QTAIM/NCI/RDG plots. Two Zn complexes selected topological parameters based on QTAIM and NCI-RDG analyses illustrated in Table 7. The QTAIM graphs and NCI-RDG iso-surfaces have been depicted in Figure 7. The study reveals that **1** is stabilized by four N···Zn interactions formed between ligands and the central zinc metal and H···N interactions between ligands. The first interactions exhibit significant binding energies ($\mathcal{E}(r) = \frac{\mathcal{V}(r)}{2}$[36] of approximately −16.50, −18.22, −16.43, and −18.22 kcal/mol, respectively. These findings indicate the robust stability and atomic organization of this compound, highlighting the potential electronic charge transfer occurring between the Zn and

https://doi.org/10.1021/acsomega.4c09312
ACS Omega 2025, 10, 14770−14786

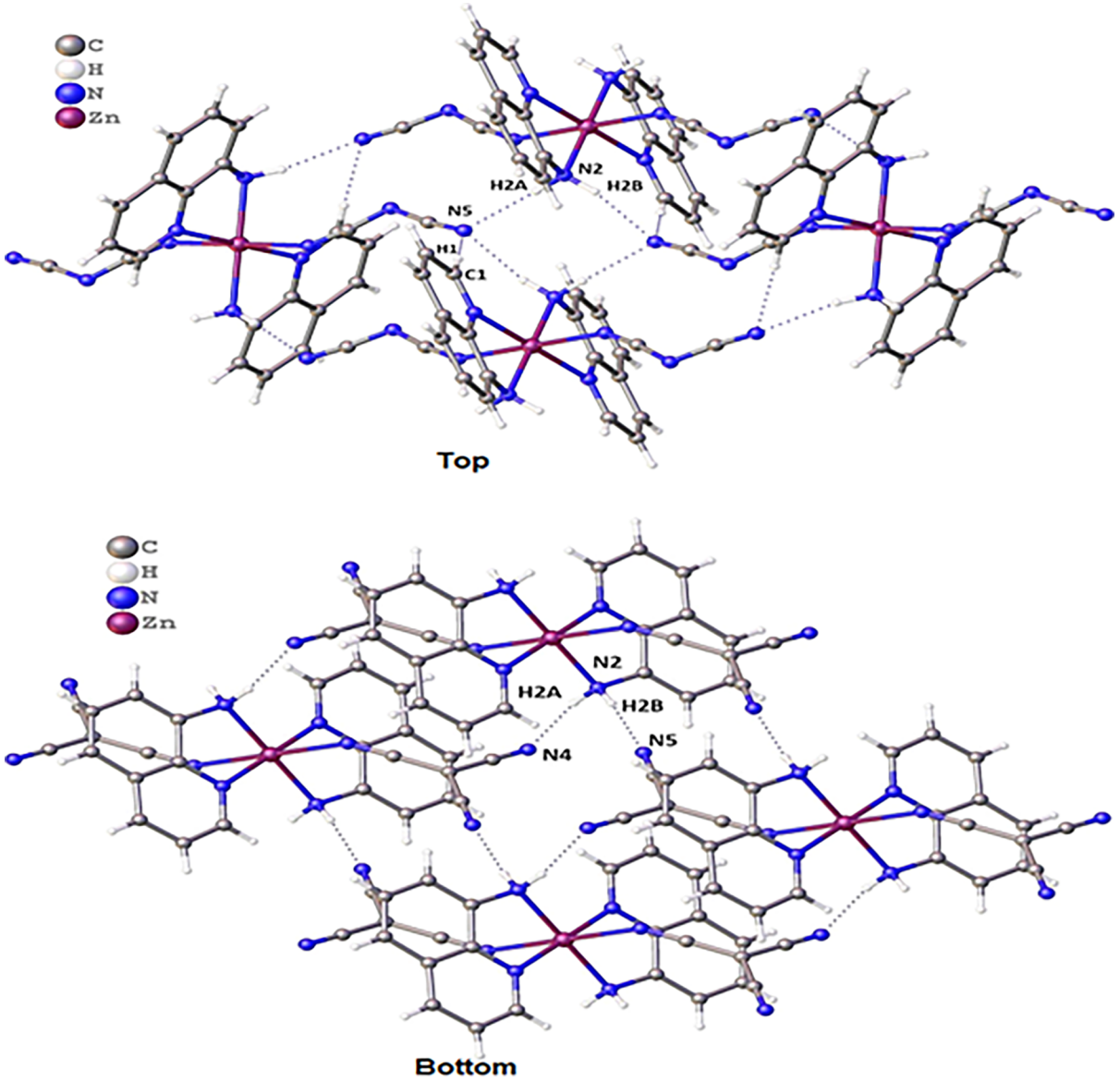

Figure 2. Perspective view of intermolecular hydrogen bonding interaction in complex **1** (top), and complex **2** (bottom) with selective atom numbering scheme.

Table 3. Hydrogen Bond Distances (Å) and Angles (°) of Complex 1

D-H···A	D-H	H···A	D···A	∠D-H···A
N(2)-H(2B)···N(5)[a]	0.89	2.15	3.036(5)	171
N(2)-H(2A)···N(5)[b]	0.89	2.15	3.024(6)	168
C(1)-H (1)···N(5)[c]	0.93	2.55	3.475(6)	171

D = donor; H = hydrogen; A = acceptor. [a]= x,1/2-y,1/2+z. [b]= 2-x, −1/2+y,1/2-z. [c]= x,3/2-y,1/2+z.

Table 4. Hydrogen Bond Distances (Å) and Angles (°) of Complex 2

D-H···A	D-H	H···A	D···A	∠D-H···A
N(2)-H(2A)···N(4)[a]	0.89	2.19	3.070(4)	168
N(2)-H(2B)···N(5)[b]	0.89	2.21	3.085(4)	169

D = donor; H = hydrogen; A = acceptor. [a]= 1-x, -y, -z. [b]= −1+x, y, z.

ligands, as confirmed by HOMO−LUMO analyses. The ellipticity of electron density is notably low, with values of 0.01 au and 0.03 au, further demonstrating the robust stability of these bonds with Zn, thereby contributing to the overall stability of the complex. According to Bianch et al., in the BCP2, BCP3, BCP5, and BCP6, the exceeds unity indicates the presence of hydrogen bonding interactions between N-ligands atoms and Zn metal. The appearance of a red spot in the NCI iso-surface further corroborates this. Additionally, **2** is stabilized through five interactions involving the nitrogen atoms of the ligands and the central Zn metal, along with two binds formed between nitrogen and the carbon of the ligands. In Table 5, the values of $\rho(r)/\nabla^2\rho(r)$ are notably elevated for BCP2, BCP3, BCP4, and BCP5, with positive values of 0.0493 au/0.1891 au, 0.0474 au/0.1739 au, 0.0475 au/0.0469 au, and 0.0493 au/0.1892, respectively. These results suggest a significant electronic charge distribution in these regions, indicative of potential strong interactions, further corroborated by MEP analysis. These bonding characteristics are exemplified by high E_{int} energies of −19.29, −18.51, −18.54, --19.29 kcal/mol, respectively, underscoring the stability of the complex.

https://doi.org/10.1021/acsomega.4c09312
ACS Omega 2025, 10, 14770−14786

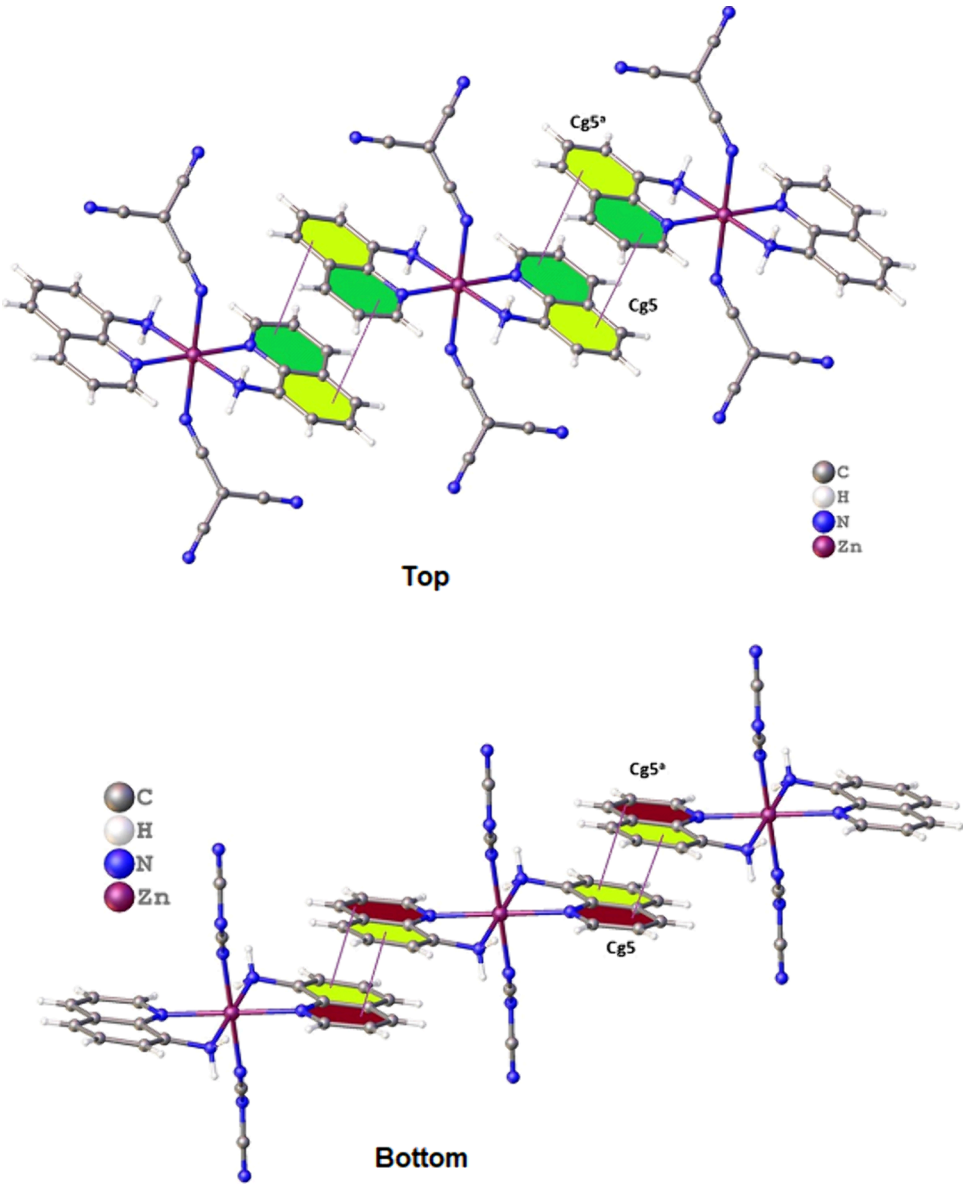

Figure 3. Perspective view of $\pi\cdots\pi$ interactions in complex **1**, symmetry elements, [a] = 1-x,1-y,1-z, (top), and in complex **2**, symmetry elements, [b] = -x,1-y,1-z (bottom).

Table 5. Geometric Features (Distances in Å and Angles in °) of the $\pi\cdots\pi$ Interactions Obtained in Both Complexes

complex	Cg(I)···Cg (J)	Cg(I)··· Perp(Å)	Cg(J)··· Perp(Å)	Cg···Cg(Å)
1	Cg (5)··· Cg(5)[a]	3.5848(15)	3.5846(15)	4.702(2)
2	Cg (5)··· Cg(5)[b]	3.5674(10)	3.5674(10)	3.6989(19)

Cg (5) = Centre of gravity of the ring [N (2)−C (1)−C (2)−C (3)−C(4)−C(9)−C(8)-C(7)−C(6)−C (5)]. Symmetry elements. [a]= 1-x,1-y,1-z; [b]= -x,1-y,1-z. α = Dihedral angle between ring I and ring J; Cg(I)···perp = perpendicular distance of Cg(I) on ring J; Cg(I)···perp = perpendicular distance of Cg(J) on ring I.

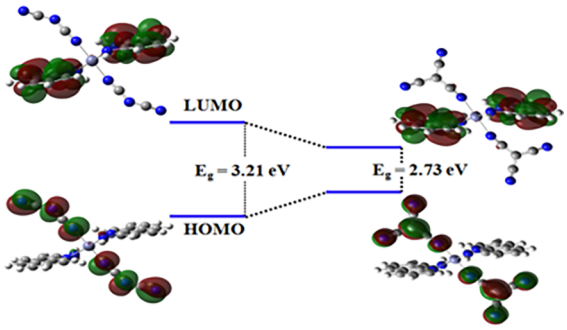

Figure 4. HOMO−LUMO iso-surface of the Zn complexes.

These bindings yield low values ranging from 0.01 au to 0.03 au, indicating well-stabilized interactions. This observation underscores the stability and atomic organization of **2**. The NCI index reveals a blue spot between N and Zn, suggesting that the ligands are anchored by HB bonding. In **2**, the RDG shows two blue peaks corresponding to sign($\lambda 2$) ρ equal to −0.04 au and −0.043 au, confirming the presence of hydrogen bonding interactions that are responsible for the complex stability, as corroborated by QTAIM analysis. Also, in **1** and **2**, the presence of green spots between ligands indicates the

https://doi.org/10.1021/acsomega.4c09312
ACS Omega 2025, 10, 14770−14786

Table 6. Energy Levels and Derived Quantum Chemical Parameters for Zn Complexes

chemical parameters (eV)	1	2
$E_g = \varepsilon_{LUMO} - \varepsilon_{HOMO}$	3.22	2.74
$IP = -\varepsilon_{HOMO}$	5.98	5.73
$EA = -\varepsilon_{LUMO}$	2.76	2.99
$\mu = -\frac{IP + EA}{2}$	−4.36	−4.35
$\chi = -\mu$	4.36	4.35
$\eta = \frac{IP - EA}{2}$	1.50	1.36
$\omega = \frac{\mu^2}{2\eta}$	6.33	6.95

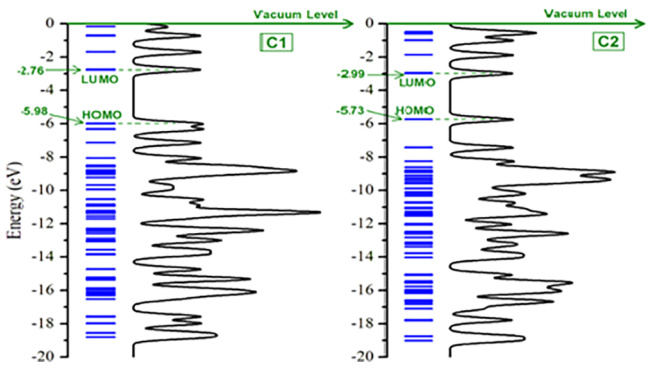

Figure 5. DOS spectra of the Zn complexes.

formation of van der Waals forces that further enhance stabilization. A comprehensive QTAIM-NCI discussion concludes that both Zn complexes are stabilizing by hydrogen bonding and van der Waals interactions. They exhibit well-organized, symmetrical, and robust stable complexes, ideally for their selected applications.

Laplacian of electron density ($\nabla^2\rho(r)$), Lagrangian kinetic energy density (G(r)), potential energy density (V(r)), ellipticity of electron density ($\varepsilon(r)$), and interaction energy ($E(r) = \frac{V(r)}{2}$)

Supramolecular R_4^4 (8)/R_2^2(16)/ R_4^4(16) Synthons: A New Crystal Engineering Concept. We expanded the QTAIM/NCI Plots investigation to include the analysis of new supramolecular synthons R_4^4 (8)/R_2^2(16)/R_4^4(16) because two X-ray structures of Zn compounds showcase unique supramolecular building blocks. Partial views of Zn compounds X-ray structures explore supramolecular interactions that result in the formation of R_4^4 (8) and R_2^2(16) synthons (**1**), and R_2^2(16)/R_4^4(16) synthons (**2**). The DFT study focuses on analyzing the strong NH···N (anionic ligand) hydrogen bonds observed in the solid-state structures of **1** and **2**, which are crucial for the formation of 2D supramolecular assemblies (Figure 8a-b). In **1**, two symmetrically independent hydrogen bonds are formed between the hydrogen atoms of the coordinated amino groups on the 8-aminoquinoline ligand and the noncoordinated nitrogen atom of the anionic coligand, dicyanamide, with H-bond distances of approximately 2.15 Å. These interactions result in the formation of R_4^4 (8) and R_2^2(16) synthons, which drive the propagation of the Zn(II) octahedral complex into 2D assemblies (Figure 8a). Similarly, in **2**, two symmetrically independent hydrogen bonds (with H-bond distances of ∼ 2.21 Å) are depicted as dashed bonds in Figure 8b. These bonds generate self-assembled dimers (denoted as A and B in Figure 8b), which correspond to R_2^2(16) synthons. The alternating propagation of these synthons leads to the 2D assembly of **2** (Figure 8b), along with the formation of a fused R_4^4(16) synthon.

Figure 9 (top) divulges the QTAIM/NCI Plot of the R_2^2(16) synthon in **1**. The interaction NH···N involves a bond critical point (BCP), a red sphere, and a bond path submitted as a dashed line—similarly, a blue reduced density gradient (RDG) iso-surface. The analysis indicates the presence of an additional CH···N interaction, as evidenced by a BCP, bond path, and a green RDG iso-surface. It suggests a weaker interaction compared to others. Unexpectedly, the QTAIM/NCI Plot analysis also identifies three BCPs, bond paths, and an extended RDG iso-surface connecting the dca coligands, indicating a weak van der Waals interaction, as the electron density at these BCPs is less than 0.004 au The interaction energy computed for the dimer is significant at − 29.2 kcal/mol, driven by the two strong NH···N hydrogen bonds, the weaker CH···N interaction, and the π(dca)···π(dca) stacking interaction. This vital interaction energy correlates with the large MEP values at the hydrogen bond donor and acceptor groups and reinforces the structure-directing role of the NH···N contacts. Figure 9 (bottom) presents a similar analysis for **2**, focusing on the two self-assembled dimers described in Figure 9b. In dimer A, the distribution of bond critical points (BCPs), bond paths, and reduced density gradient (RDG) iso-surfaces is like that observed in **1**, with blue RDG iso-surfaces characterizing the vital NH···N hydrogen bonds. Additionally, two symmetrically equivalent CH···N contacts are present, involving the CH groups ortho to the pyridinic nitrogen atom,

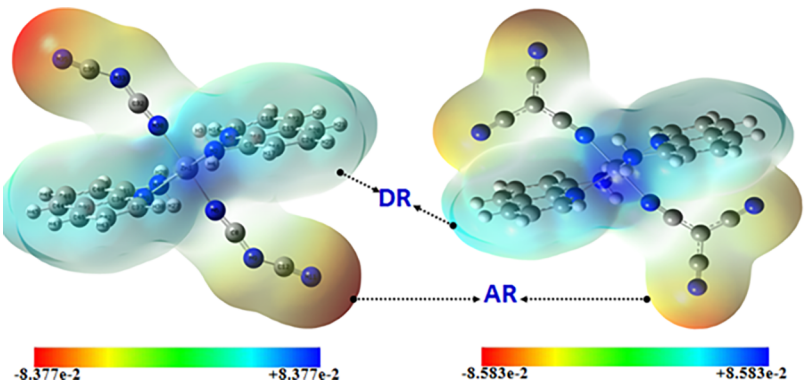

Figure 6. MEP iso-surface of the Zn complexes (AR: acceptor Region and DR: Donor Region).

https://doi.org/10.1021/acsomega.4c09312
ACS Omega 2025, 10, 14770−14786

Table 7. Topological QTAIM Parameters at Selected Bond Critical Points (BCPs)

complexes	BCPs	$\rho(r)$	$\nabla^2\rho(r)$	G(r)	V(r)	$\frac{\lvert V(r)\rvert}{G(r)}$	$\varepsilon(r)$	E_{int} (kcal/mol)
(1)	1	0.0160	0.0695	0.0145	−0.0117	0.80	1.05	−3.66
	2	0.0427	0.1502	0.0416	−0.0526	1.26	0.01	**-16.50**
	3	0.0467	0.1777	0.0469	−0.0581	1.23	0.03	**-18.22**
	4	0.0160	0.0695	0.0145	−0.0117	0.80	1.05	−3.66
	5	0.0427	0.1502	0.0416	−0.0526	1.26	0.01	**-16.43**
	6	0.0467	0.1777	0.0469	−0.0581	1.23	0.03	**-18.22**
(2)	1	0.0025	0.0078	0.0014	−0.0008	0.57	0.94	−0.25
	2	0.0493	0.1891	0.0496	−0.0615	0.23	0.03	**-19.29**
	3	0.0474	0.1739	0.0469	−0.0590	1.25	0.01	**-18.51**
	4	0.0475	0.1740	0.0469	−0.0591	1.26	0.01	**-18.54**
	5	0.0493	0.1892	0.0496	−0.0615	1.23	0.03	**-19.29**
	6	0.0025	0.0078	0.0014	−0.0008	0.57	0.97	−0.25

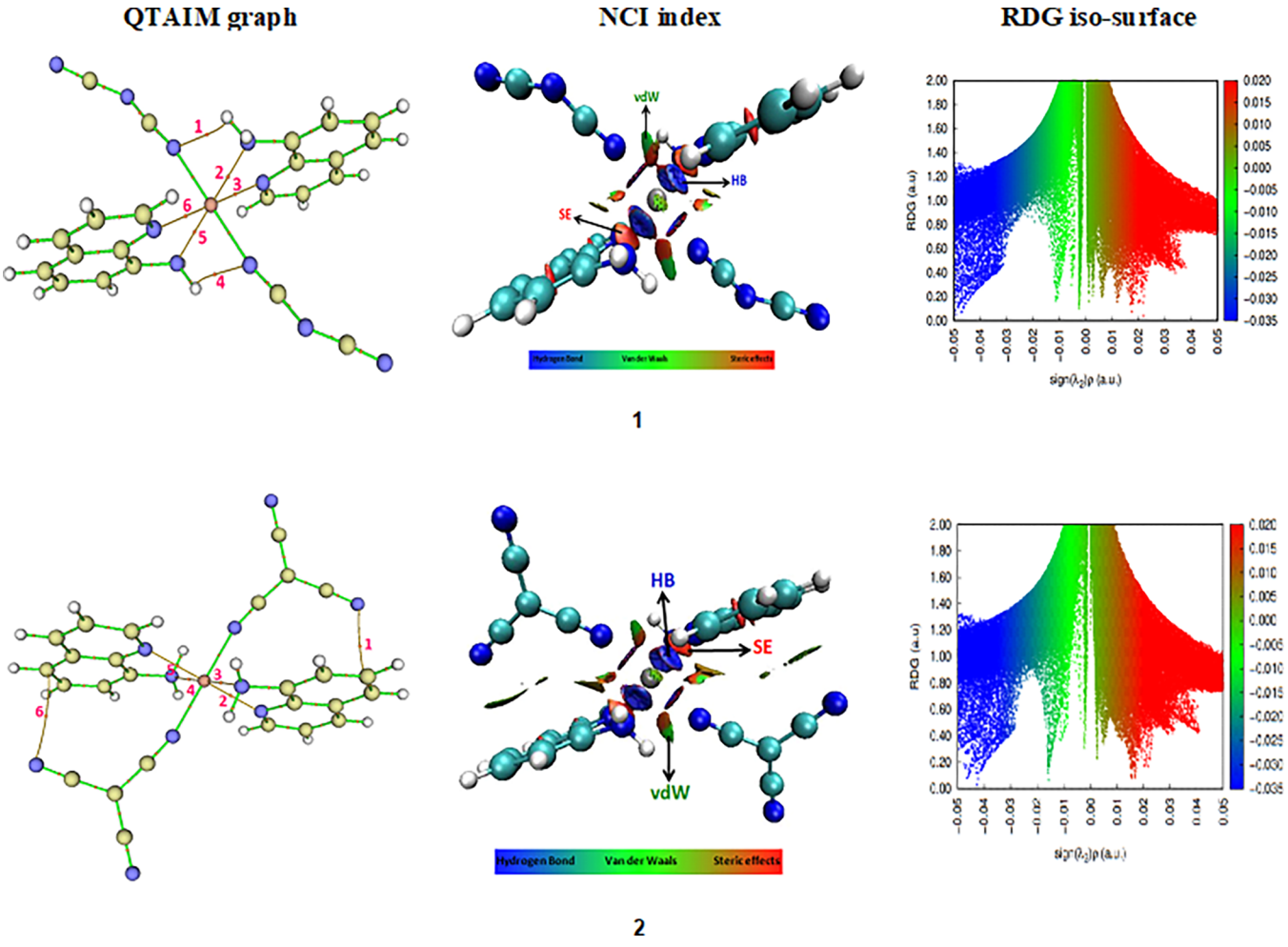

Figure 7. QTAIM and NCI-RDG analyses for Zn complexes.

as confirmed by the QTAIM/NCI Plot analysis. A BCP and bond path also interconnect two CN groups of the TCM anions, indicating the presence of antiparallel CN···CN contacts, which can be classified as $\pi\cdots\pi$ interactions, as previously demonstrated.[37] The interaction energy of this dimer (Figure 9a) is − 30.8 kcal/mol, comparable to the $R_2^2(16)$ synthon of **1** due to a similar combination of noncovalent interactions. Dimer B (Figure 9b) exhibits a slightly lower dimerization energy (−28.0 kcal/mol), most likely due to the absence of ancillary CH···N hydrogen bonds. Unlike in dimer A, TCM···TCM contacts are not observed. Instead, the tcm ligand of one monomer interacts with the pyridine ring of the 8-AMQ ligand in the adjacent monomer and vice versa. Two BCPs and bond paths characterize each interaction: one connects the central carbon atom of the TCM to a C atom of the Py (pyridine) ring, forming an electrostatically enhanced $\pi\cdots\pi$ contact. Instead, the C−H bond points toward the π-system of a CN group, consistent with a CH···π interaction. Additionally, one aromatic hydrogen atom of the pyridine ring is linked to the nitrogen atom of the

https://doi.org/10.1021/acsomega.4c09312
ACS Omega 2025, 10, 14770−14786

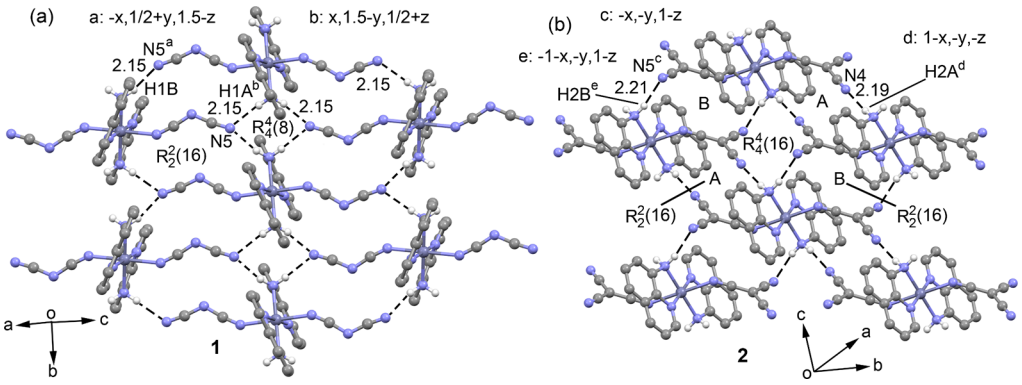

Figure 8. a-b. Partial views of the X-ray structures of compounds **1** (a) and **2** (b) Distances in Å.

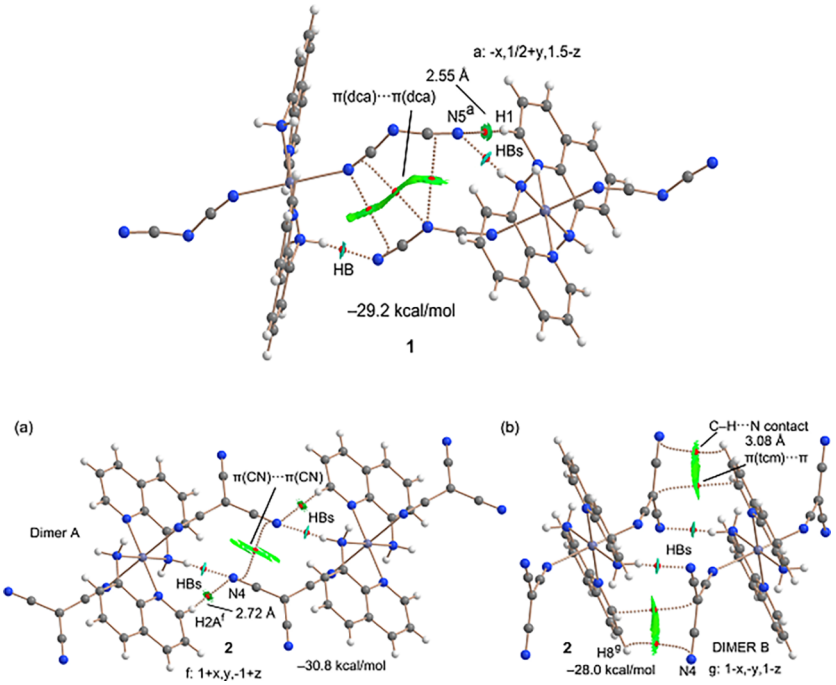

Figure 9. QTAIM (BCPs in red, bond paths as dashed bonds) and NCI Plot analysis (RDG = 0.5, ρ cutoff = 0.04 au, color range − 0.03 au ≤ (signλ_2) ρ ≤ 0.03 au, blue-green-yellow-red) of the $R_2^2(16)$ synthon of compound **1**. Only intermolecular interactions are represented (**top**), QTAIM (BCPs in magenta, bond paths as dashed bonds) and NCI Plot analysis (RDG = 0.5, ρ cutoff = 0.04 au, color range − 0.03 au ≤ (signλ2) ρ ≤ 0.03 au, blue-green-yellow-red) of dimer A (a) and B (b) of compound **2**. Only intermolecular interactions are represented (**bottom**).

tcm ligand, indicating the presence of a CH···N contact. Similar contacts involving pseudohalide ligands have been demonstrated to play a significant role in crystal engineering.[37c]

ELF-LOL Iso-surfaces. The ELF-LOL iso-surfaces are highly selective tools for investigating electronic distribution and charge transfer phenomena within the studied Zn complex.[38] ELF and LOL values range from 0 to 1 and 0.0 to 0.8, respectively. An ELF value greater than 0.5 suggests the existence of bonding, nonbonding, and localized electrons, whereas a low value corresponds to electrons being delocalized. Figure 10a-d explores the 2D-ELF and 2D-LOL profiles. In both complexes, a dark red color envelopes H21 and H45 for (**1**) (Figure 10a-b) and H27 and H53 for (**2**), (Figure 10c-d) with a maximum ELF value of 1.0. The condition shows that both electrons are bonding, and electrons are not bonding in this specific region. The LOL exhibits a blue color surrounding the nitrogen and carbon atoms and the central metal Zn, highlighting the delocalization of electrons in these regions. These results suggest potential electronic charge transfer between the ligands in their interactions with the zinc, forming a donor−acceptor pair within the structure. This idea enhances the stability of each complex through hydrogen bonding, a conclusion further supported by QTAIM analyses.

Biological Spectrum. *Cytotoxic Activity.* The synthesized compounds demonstrated significant cytotoxic activity against the DLA cell line.[29a] Among these, the Zn salt exhibited the lowest percentage of cell death (Table 8, Figure 11a). The compounds showed varying levels of cytotoxicity at different concentrations, with C**1** displaying the highest activity at lower concentrations. However, none of the synthesized compounds achieved 100% cell death at any of the concentrations tested. The data is graphically represented in Figure 11b. Using regression analysis, a linear trendline was plotted to calculate the IC_{50}. The IC_{50} measures a substance's effectiveness in inhibiting a specific biological or biochemical function. This indicates that the concentration needed to reach 50% inhibition of a biological process in vitro is required. In this

https://doi.org/10.1021/acsomega.4c09312
ACS Omega 2025, 10, 14770−14786

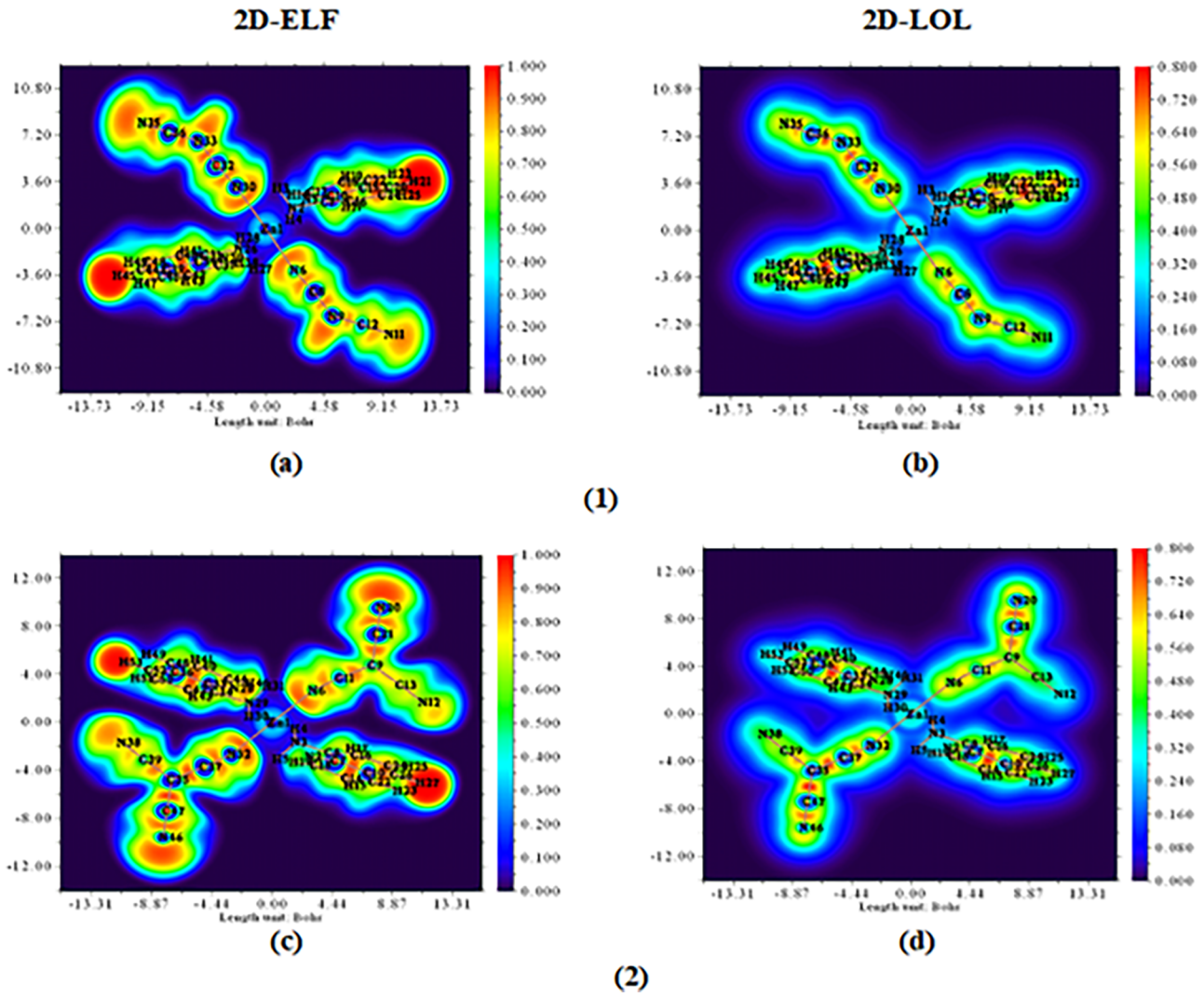

Figure 10. a-d. Zn complexes 2D-ELF and 2D-LOL analyses.

Table 8. (%) Cell Death after Exposure to Different Concentrations of Compounds

drug concentration (μg/mL)	% cell death			
	8-AMQ	Zn salt	C1	C2
12.5	3.7 ± 0	4.46 ± 2.1	19.9 ± 2.6	11.9 ± 1.5
25	7.88 ± 1.5	7.06 ± 1.5	29.5 ± 0.8	16.5 ± 1.7
50	13.6 ± 1.2	9.53 ± 1.6	40.4 ± 1.6	24.3 ± 2.6
100	21.2 ± 1.6	13.6 ± 0.7	60.4 ± 1.8	33.3 ± 0.6
150	30.1 ± 1.1	17.6 ± 2.8	68.1 ± 1.3	48.2 ± 1.7
200	37.5 ± 1.4	29.6 ± 2.6	76.5 ± 1.1	60.7 ± 2.7

[Control tube contains 5 dead cells, Sample dissolves in DMSO].

study, the IC_{50} was 92.53 μg/mL. The results show the percentage of cell death in the DLA cell line at drug concentrations from 12.5 μg/mL to 200 μg/mL. The compound labeled 8-AMQ displayed 3.7% inhibition of cytotoxicity at a concentration of 12.5 μg/mL, whereas the Zn salt exhibited 4.46% inhibition at the same concentration. For 8-AMQ, the percentages of cell death increased to 7.88%, 13.6%, 21.2%, 30.1%, and 37.5% at concentrations of 25, 50, 100, 150, and 200 μg/mL. The Zn salt-induced cell death rates of 12.5%, 25%, 50%, 100%, 150%, and 200% at concentrations of 4.46, 7.06, 9.53, 13.6, 17.6, and 29.6 μg/mL. C**1**'s cell death percentages were 19.9%, 29.5%, 40.4%, 60.4%, 68.1%, and 76.5% at concentrations of 12.5, 25, 50, 100, 150, and 200 μg/mL, respectively. The most significant cytotoxic impact occurred when C1 was administered at a 200 μg/mL concentration, leading to a 76.5% decrease in cell viability. At the same concentration, C**2** showed 60.7% inhibition of cell viability. The study concludes that while all synthesized compounds are effective against DLA solid cells, C**1** is the most effective, indicating its potential as a promising anticancer agent.

Structure–Activity Relationship. The cytotoxicity results revealed a significant finding that the percentage of cell viability decreased cumulatively with increasing concentrations of the investigated complexes. The higher concentrations of the compound resulted in a decrease in the percentage of viable cells. The cytotoxicity behavior of the Zn complexes has been lucidly explained based on SAR (Structure–Activity-Relationship) governed by factors like the -NH_2 group, Zn metal, and X ions nature (X = dca (**1**)/TCM (**2**). Our synthesized complexes are mononuclear, involving -NH_2 group ligand, Zn ions in contact with X. The cytotoxicity results displayed that **1** showed greater effectiveness than **2**, as evidenced by the

https://doi.org/10.1021/acsomega.4c09312
ACS Omega 2025, 10, 14770−14786

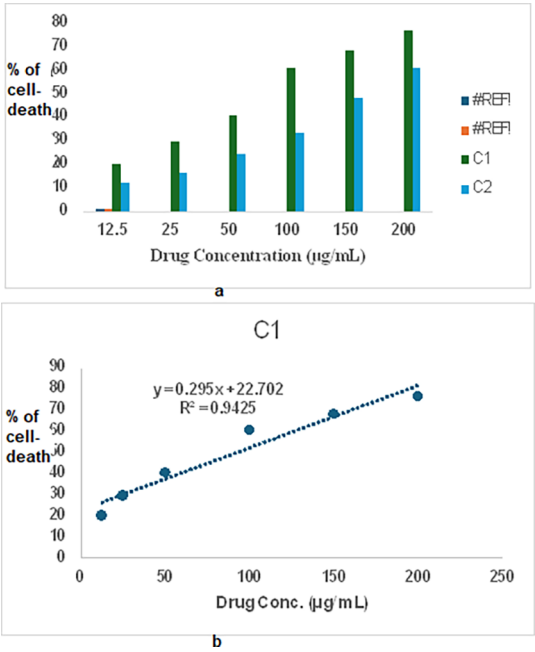

Figure 11. a-b. (a) Cell death percentage (%) after exposure to different concentrations of C**1**-C**2** and (b) Linear regression analysis for the % cell death of C**1** against DLA.

lower percentage of cell death in the DLA cells. The role of Zn in respiration, energy metabolism, and DNA synthesis is a crucial aspect of our research, with zinc serving a structural role in these proteins.[39] Several metal complexes, including platinum, have been proven to hinder the growth of cancer cells. In cytotoxic activity, at least one amino ($-NH_2$) derivative group is essential for hydrogen bonding to DNA. The activity was linked to fewer hydrogen bonds forming between the ligands and DNA bases as the number of N−H groups in the ligands decreased. One way to modify the physicochemical properties is to change the ligands on the metal center, which can improve compound uptake.[39] Further, the leaving group's nature affects toxicity; reactive leaving groups increase toxicity, while stable, poor leaving groups reduce reactivity toward DNA.[39] Moreover, there is a link between the electronic effects of substituent ions (X) and their cytotoxicity against DLA cell lines. In the synthesized Zn complexes, X are dca and TCM. The two ligands structurally differ mainly due to one CN additional group in TCM, which probably alters the cytotoxicity results.[39]

Photodynamic Antifungal Therapy. APDT with the synthesized Zn complexes showed significant activity against *C. albicans*, as indicated by their zones of inhibition (Figure S18a-b), with increased effectiveness upon irradiation. The samples exposed to radiation, C1* and C**2**, exhibited a growth in zone diameter of around 15 mm concerning each strain. The results demonstrate the efficacy of our adapted drug system for photodynamic therapy (APDT)/PACT. The irradiated samples exhibited substantial activity against *C. albicans*, with zone diameters of 22.21 ± 1 mm for C**1*** and 47.20 ± 3 mm for C**2***. The research revealed that the highly susceptible strains to our PDT studies resisted the antibiotic griseofulvin, demonstrating no inhibition zone against either strain. The antifungal activity mechanisms include membrane disruption, cell cycle arrest, and ROS-dependent fungal cell death. The photosensitizer (PS) in an excited state can generate highly active substances that have the potential to damage microbial cells through type-I or type-II mechanisms. The MIC values determined through PDT are listed in Table 9, with the MIC value being 2.5 μg/mL for each strain. The results are comparable to the literature published d^{10} complexes.[40]

Table 9. Antifungal Zones of Inhibition and MIC Values of PACT

fungal strain *C. albicans*	zone of inhibition ± standard deviation (mm)	MIC (μg/mL)
C**1***	22.21 ± 1	2.5
C**2***	47.20 ± 3	2.5

CONCLUSION

In conclusion, we synthesized 8-aminoquinoline-based Zn complexes with dicyanamide and tricyanomethane anions. The complexes are structurally characterized using various analytical methods, including NMR, PXRD, SCXRD, and XPS techniques. The X-ray single-crystal structure revealed that the complex crystallizes in the monoclinic and triclinic space groups, $P21/c$ and P-1, and crystal-packing divulge N−H···N bonds as well as weak C−H···N interactions. Hirshfeld surface and fingerprint plots quantitatively ensure that complexes exhibit different supramolecular interactions, including pi···pi stacking. DFT studies confirmed that **2** has more conductivity and reactivity properties. QTAIM/NCI-RDG plot confirms N···Zn/H···N interactions and explored new supramolecular $R_4^4(8)/R_2^2(16)$ crystallographic synthons. The dose-dependent cytotoxicity of two Zn complexes was evaluated against the DLA cell line. The results indicated that **1** showed greater effectiveness than **2**, as evidenced by the lower percentage of cell death in the DLA cells. The findings suggest that complex **1** is a potential candidate for cancer therapy. The antifungal photodynamic therapy study showed notable effectiveness against *C. albicans*, with 22.21 ± 1 mm and 47.20 ± 3 mm zone diameters. The article presents significant findings on the X-ray crystal structure, highlighting new supramolecular synthons and $\pi\cdots\pi$ stacking interactions at a large Cg···Cg distances enhance our understanding of the complex's structural properties.

ASSOCIATED CONTENT

Supporting Information

The Supporting Information is available free of charge at https://pubs.acs.org/doi/10.1021/acsomega.4c09312.

Figures for HRMS, IR/Raman, UV−vis, $^1H/^{13}C$ NMR, PXRD, SEM, MEP, APDT experiments and graphs, Tables for EDX, and XPS spectral data, NBO calculations, Scheme for DCA/TCM bridging propensity, Hirshfeld surface and 2D fingerprint plot, NBO/QTAIM/NCI-RDG basic principle (PDF)

Accession Codes

CCDC 2379762−2379763 contain the supplementary crystallographic data for this paper. These data can be obtained free of charge via www.ccdc.cam.ac.uk/data_request/cif, or by emailing data_request@ccdc.cam.ac.uk, or by contacting The Cambridge Crystallographic Data Centre, 12 Union Road, Cambridge CB2 1EZ, UK; fax: + 44 1223 336033.

https://doi.org/10.1021/acsomega.4c09312
ACS Omega 2025, 10, 14770−14786

AUTHOR INFORMATION

Corresponding Authors

Dhrubajyoti Majumdar − *Department of Chemistry, Tamralipta Mahavidyalaya, Tamluk, West Bengal 721636, India*; orcid.org/0000-0002-9785-7750; Email: dmajumdar30@gmail.com

Sudipta Dalai − *Department of Chemistry and Chemical Technology, Vidyasagar University, Midnapore, West Bengal 721102, India*; Email: sudipta@mail.vidyasagar.ac.in

Authors

Suman Hazra − *Department of Chemistry, Tamralipta Mahavidyalaya, Tamluk, West Bengal 721636, India; Department of Chemistry and Chemical Technology, Vidyasagar University, Midnapore, West Bengal 721102, India*

Jessica Elizabeth Philip − *Department of Chemistry, St. George's College, Kottayam, Kerala 686122, India*

Bouzid Gassoumi − *Laboratory of Advanced Materials and Interfaces (LIMA), Faculty of Sciences of Monastir, Avenue of Environment, University of Monastir, Monastir 5000, Tunisia*

Antonio Frontera − *Department de Quimica, Universitat de les Illes Balears, Palma de Mallorca (Baleares) 07122, Spain*; orcid.org/0000-0001-7840-2139

Sourav Roy − *Solid State and Structural Chemistry Unit, Indian Institute of Science, Bangalore 560 012, India*

Houcine Ghalla − *Quantum and Statistical Physics Laboratory, Faculty of Science, University of Monastir, Monastir 5079, Tunisia*

Complete contact information is available at: https://pubs.acs.org/10.1021/acsomega.4c09312

Author Contributions

Suman Hazra is involved in formal analysis, research investigation, literature survey, writing review, draft editing, Graphics preparation, and software visualization. **Dr. Dhrubajyoti Majumdar** was the project's author and conceived the whole research idea, performed data curation, conceptualization, methodology, research investigation, formal analysis, contributed reagents, materials, software visualization, writing review, initial draft preparation, and editing. **Dr. Jessica Elizabeth Philip** performed formal analysis, research investigation, biological study, and software visualization. **Dr. Bouzid Gassoumi** and **Dr. Houcine Ghalla** performed DFT experiments. **Prof. Dr. A. Frontera** performed DFT experiments. **Dr. Sourav Roy** was involved in X-ray crystallographic work. **Prof. Dr. Sudipta Dalai** supervises conceptualization, methodology, research investigation, and formal analysis. All authors reviewed and approved the final version of the manuscript before its submission.

Notes

The authors declare no competing financial interest.

ACKNOWLEDGMENTS

The research study has not received funding from any public, commercial, or nonprofit organization. The authors thank the Central Laboratory of Tamralipta Mahavidyalaya, Tamluk, and the Department of Chemistry and Chemical Technology Vidyasagar University, Midnapore, West Bengal, India, for their support. We conducted advanced instrumental analyses at STIC, Cochin, SAIC Tezpur University, and CIF, IIT Jammu, India. We thank these institutions and Amala Cancer Research Centre, Kerala, for the cytotoxicity studies.

REFERENCES

(1) (a) Ruankham, W.; Songtawee, N.; Prachayasittikul, V.; Worachartcheewan, A.; Suwanjang, W.; Pingaew, R.; Prachayasittikul, V.; Prachayasittikul, S.; Phopin, K. Promising 8-Aminoquinoline-Based Metal Complexes in the Modulation of SIRT1/3-FOXO3a Axis against Oxidative Damage-Induced Preclinical Neurons. *ACS Omega* **2023**, *8*, 46977−46988. (b) Prachayasittikul, V.; Prachayasittikul, S.; Ruchirawat, S.; Prachayasittikul, V. 8-Hydroxyquinolines: A review of their metal chelating properties and medicinal applications. *Drug Des Devel Ther.* **2013**, *7*, 1157−1178. (c) Kim, Y.; Kim, S.-J.; Choi, S. H.; Han, J. H.; Nam, S. H.; Lee, J. H.; Kim, H. J.; Kim, C.; Kim, D. W.; Jang, H. G. Crystal structures and catalytic activities of Zn(II) compounds containing 1,3-bis(4-pyridyl)propane. *Inorg. Chim. Acta* **2006**, *359*, 2534−2542.

(2) (a) Mirzaei, M.; Eshtiagh-Hosseini, H.; Bolouri, Z.; Rahmati, Z.; Esmaeilzadeh, A.; Hassanpoor, A.; Bauza, A.; Ballester, P.; Barceló-Oliver, M.; Mague, J. T.; Notash, B.; Frontera, A. Rationalization of Noncovalent Interactions within Six New MII/8-Aminoquinoline Supramolecular Complexes (MII = Mn, Cu, and Cd): A Combined Experimental and Theoretical DFT Study. *Cryst. Growth Des.* **2015**, *15*, 1351−1361. (b) Amiri, A.; Mirzaei, M. *Metal−Organic Frameworks in Analytical Chemistry*; Royal Society of Chemistry: 2023. . (c) Udhayakumari, D.; Ramasundaram, S.; Jerome, P.; Oh, T. H. A Review on Small Molecule Based Fluorescence Chemosensors for Bioimaging Applications. *J. Fluoresc.* **2024**, 1−25. (d) Li, Y.; Nguyen, M.; Vendier, L.; Robbert, A.; Liu, Y.; Meunier, B. X-Ray diffraction structure of Cu(II) and Zn(II) complexes of 8-aminoquinoline derivatives (TDMQ), related to the activity of these chelators as potential drugs against Alzheimer's disease. *J. Mol. Struct.* **2022**, *1251*, No. 132078. (e) Gole, M. T.; Pauls, P.; Hartlaub, S. F.; Nataro, C.; Rossiter, L. M.; O'Connor, A. R.; Chan, B. C. Synthesis and electronic properties of transition metal complexes containing sulfonamidoquinoline ligands. *Polyhedron* **2021**, *205*, No. 115269. (f) Mautner, F. A.; Fischer, R. C.; Torvisco, A.; Salem, N. M. H.; Dugas, A. R.; Aaron, S. F.; Sahu, S. P.; Louka, F. R.; Massoud, S. S. Stereochemical Geometries and Photoluminescence in Pseudo-Halido-Zinc(II) Complexes. Structural Comparison between the Corresponding Cadmium(II) Analogs. *Inorganics* **2021**, *9*, 53. (g) Rehman, F.; Zafar, M. N.; Yousuf, S.; Nazar, M. F.; Mughal, E. U.; Malik, A.; Sumrra, S. H.; Zafar, M. N.; Rafique, H. Zn(II) Complexes with Quinoline Supported Amidate Ligands:Synthesis, Fluorescence, and Catalytic Activity. *Russian Journal of General Chemistry* **2019**, *89*, 2516−2521. (h) Deraeve, C.; Maraval, A.; Vendier, L.; Faugeroux, V.; Pitié, M.; Meunier, B. Preparation of New Bis(8-aminoquinoline) Ligands and Comparison with Bis(8-hydroxyquinoline) Ligands on Their Ability to Chelate CuII and ZnII. *Eur. J. Inorg. Chem.* **2008**, *2008*, 5622−5631. (i) Baruah, A. M.; Sarma, R.; Baruah, J. B. A penta-coordinated bis-(8-aminoquinoline) monobenzoato zinc(II) benzoate complex favored by self-assembly formation. *Inorg. Chem. Commun.* **2008**, *11*, 121−124. (j) Paira, M. K.; Dinda, J.; Lu, T. -H; Paital, A. R.; Sinha, C. Zn(II), Cd(II) and Hg(II) complexes of 8-aminoquinoline: Structure, spectra and photoluminescence property. *Polyhedron* **2007**, *26*, 4131−4140.

(3) (a) Pingaew, R.; Worachartcheewan, A.; Prachayasittikul, V.; Prachayasittikul, S.; Ruchirawat, S.; Prachayasittikul, V. Transition metal complexes of 8-aminoquinoline-5-substituted uracils with antioxidative and cytotoxic activities. *Lett. Drug Des Discovery* **2013**, *10* (9), 859−864. (b) Sinthupoom, N.; Prachayasittikul, V.; Pingaew, R.; Worachartcheewan, A.; Prachayasittikul, S.; Ruchirawat, S.; Prachayasittikul, V. Copper complexes of 8-aminoquinoline and uracils as novel aromatase inhibitors. *Lett. Drug Des. Discovery* **2017**, *14* (8), 880−884.

(4) Kerr, M. C.; Preston, H. S.; Ammon, H. L.; Huheey, J. E.; Stewart, J. M. The crystal structure of trans-bis(8-aminoquinoline) aqua zinc(II)tetracholorozincate(II). *J. Coord. Chem.* **1981**, *11*, 111−115.

https://doi.org/10.1021/acsomega.4c09312
ACS Omega 2025, 10, 14770−14786

(5) Lehn, J.-M. *Supramolecular Chemistry: Concepts and Perspectives*; VCH: Weinheim, 1995.
(6) (a) Eshtiagh-Hosseini, H.; Mirzaei, M.; Zarghami, S.; Bauzá, A.; Frontera, A.; Mague, J. T.; Habibi, M.; Shamsipur, M. Crystal engineering with coordination compounds of 2,6-dicarboxy-4-hydroxypyridine and 9-aminoacridine fragments driven by different nature of the face-to-face $\pi\cdots\pi$ stacking. *CrystEngComm* **2014**, *16*, 1359−1377. (b) Hong, M. C.; Zhao, Y. J.; Su, W. P.; Cao, R.; Fujita, M.; Zhou, Z. Y.; Chan, A. S. C. A Nanometer-Sized Metallo-supramolecular Cube with Oh Symmetry. *J. Am. Chem. Soc.* **2000**, *122*, 4819−4820. (c) Aakeröy, C. B.; Champness, N. R.; Janiak, C. Recent advances in crystal engineering. *CrystEngComm* **2010**, *12*, 22−43. (d) Sertphon, D.; Harding, D. J.; Harding, P.; Adams, H. Effect of the b-diketonate ligand on the spin states of $[Ni(b\text{-}dkt)_2(NH_2\text{-}quin)]$ complexes. *Polyhedron* **2011**, *30*, 2740−2745. (e) Genre, C.; Jeanneau, E.; Bousseksou, A.; Luneau, D.; Borshch, S. A.; Matouzenko, G. S. First dicyanamide-bridged spin-crossover coordination polymer: Synthesis, structural, magnetic, and spectroscopic studies. *Chem. - Eur. J.* **2008**, *14*, 697−705. (f) Khavasi, H. R.; Mohammad Sadegh, B. M. Temperature-Dependent Supramolecular Motif in Coordination Compounds. *Inorg. Chem.* **2010**, *49*, 5356−5358. (g) Withersby, M. A.; Blake, A. J.; Champness, N. R.; Cooke, P. A.; Hubberstey, P.; Li, W.-S.; Schroder, M. Solvent Control in the Synthesis of 3,6-Bis(pyridin-3-yl)-1,2,4,5-tetrazine-Bridged Cadmium-(II) and Zinc(II) Coordination Polymers. *Inorg. Chem.* **1999**, *38*, 2259−2266. (h) Blake, A. J.; Brooks, N. R.; Champness, N. R.; Cooke, P. A.; Deveson, A. M.; Fenske, D.; Hubberstey, P.; Schroder, M. Controlling copper (I) halide framework formation using N-donor bridging ligand symmetry: use of 1, 3, 5-triazine to construct architectures with threefold symmetry. *J. Chem. Soc., Dalton Trans.* **1999**, 2103−2110.
(7) (a) Dong, W.; Wang, Q.-L; Liu, Z.-Q; Liao, D.-Z; Jiang, Z.-H; Yan, S.-P; Cheng, P. Syntheses, structures and magnetic properties of 1-D complex $\{[Ni(\mu_{1,5}\text{-}dca)(pn)_2](ClO_4)\}_n$, 2-D complex $[Mn(\mu_{1,5}\text{-}dca)_2(phen)]_n$ and 3-D complex $[Mn(\mu_{1,5}\text{-}dca)_2L]_n$ (dca = dicyanamide, $N(CN)_2^-$; pn = 1,3-propane diamine; phen = phenanthroline; L = 4,4′-ditriazole methane). *Polyhedron* **2003**, *22*, 3315−3319. (b) Hazra, S.; Majumdar, D.; Philip, J. E.; Gassoumi, B.; Ghalla, H.; Roy, S.; Dalai, S. Dicyanamide Anion Protracted Assemblies of Cd(II)-Salen Type Coordination Polymers: Synthetic Perspective, Characterization, Crystallographic Notability, DFT Overview, and Biological Appraisal. *J. Inorg. Organomet. Polym. Mater.* **2024**, *35*, 661. (c) Majumdar, D. J.; Philip, J. E.; Tuzun, B.; Roy, S. Synthesis, characterization, crystallographic aspects, Fukui function, and photodynamic antifungal chemotherapy investigation of Cd(II)-tricyanomethanide coordination polymer: Insights from DFT. *Inorg. Chem. Commun.* **2023**, *155*, No. 111057. (d) Majumdar, D.; Dey, S.; Kumari, A.; Pal, T. K.; Bankura, K.; Mishra, D. Dicyanamide-intertwined assembly of two new Zn complexes based on N_2O_4-type pro-ligand: Synthesis, crystal networks, spectroscopic insights, and selective nitroaromatic turn-off fluorescence sensing. *Spectrochim. Acta, Part A* **2021**, *254*, No. 119612. (e) Majumdar, D.; Agrawal, Y.; Thommas, R.; Ullah, Z.; Santra, M. K.; Das, S.; Pal, T. K.; Bankura, K.; Mishra, D. Syntheses, characterizations, crystal structures, DFT/TD-DFT, luminescence behaviours and cytotoxic effect of bicompartmental Zn (II)-dicyanamide Schiff base coordination polymers: An approach to apoptosis, autophagy and necrosis type classical cell death. *Appl. Organomet. Chem.* **2020**, *34*, No. e5269. (f) Majumdar, D.; Das, S.; Thommas, R.; Ullah, Z.; Sreekumar, S. S.; Das, D.; Shukla, P.; Bankura, K.; Mishra, D. Syntheses, X-ray crystal structures of two new Zn(II)-dicyanamide complexes derived from H2vanen-type compartmental ligands: Investigation of thermal, photoluminescence, in vitro cytotoxic effect and DFT-TDDFT studies. *Inorg. Chim. Acta* **2019**, *492*, 221−234. (g) Jones, L. F.; Dea, L. O.; Offermann, D. A.; Jensen, P.; Moubaraki, B.; Murray, S. K. Benzotriazole based 1-D, 2-D and 3-D metaldicyanamide andtricyanomethanide coordination networks. *Polyhedron* **2006**, *25*, 360−372.
(8) (a) Kohout, J.; Jäger, L.; Hvastijova, M.; Kožíšek, J. Tricyanomethanide and Dicyanamide Complexes of Cu(II), Ni(II), Co(II), Their Structures and Properties. *J. Coord. Chem.* **2000**, *51*, 169−218. (b) Chemistry of pseudohalides. In *Topics in inorganic and general chemistry*; Eds.: Golub, A. M; Ghler, H. K; Skopenko, V. V.; Elsevier: Amsterdam, 1983, *21*, 413−454.
(9) Majumdar, D. J.; Frontera, A.; Roy, S.; Sutradhar, D. Experimental and Theoretical Survey of Intramolecular Spodium Bonds/σ/π-Holes and Noncovalent Interactions in Trinuclear Zn(II)-Salen Type Complex with OCN^- Ions: A Holistic View in Crystal Engineering. *ACS Omega* **2024**, *9*, 1786−1797.
(10) Hazra, S.; Majumdar, D.; Frontera, A.; Roy, S.; Gassoumi, B.; Ghalla, H.; Dalai, S. On the Significant Importance of Hg···Cl Spodium Bonding/σ/π-Hole/Noncovalent Interactions and Nano-Electronic/Conductivity Applications in Mercury Complexes: Insights from DFT Spectrum. *Cryst. Growth Des.* **2024**, *24*, 7246−7261.
(11) (a) Joshi, T.; Graham, B.; Spiccia, L. Macrocyclic Metal Complexes for Metalloenzyme Mimicry and Sensor Development. *Acc. Chem. Res.* **2015**, *48*, 2366−2379. (b) Basak, T.; Bhattacharyya, A.; Das, M.; Harms, K.; Bauzá, A.; Frontera, A.; Chattopadhyay, S. Phosphatase Mimicking Activity of Two Zinc(II) Schiff Base Complexes with Zn_2O_2 Cores: NBO Analysis and MEP Calculation to Estimate Non-Covalent Interactions. *ChemistrySelect* **2017**, *2*, 6286−6295. (c) Karmakar, M.; Chattopadhyay, S. Visible light driven photodegradation of methylene blue with two reduced Schiff base complexes of zinc(II): Exploration of their phosphatase mimicking ability. *Polyhedron* **2020**, *184*, No. 114527. (d) Tirel, E. Y.; Bellamy, Z.; Adams, H.; Lebrun, V.; Duarte, F.; Williams, N. H. Catalytic zinc complexes for phosphate diester hydrolysis. *Angew. Chem., Int. Ed.* **2014**, *53*, 8246−8250.
(12) Basak, T.; Frontera, A.; Chattopadhyay, S. Synthesis and characterization of a mononuclear zinc(II) Schiff base complex: on the importance of C−H···π interactions. *RSC Adv.* **2021**, *11*, 30148−30155.
(13) Majumdar, D. J.; Dubey, A.; Tufail, A.; Sutradhar, D.; Roy, S. Synthesis, spectroscopic investigation, molecular docking, ADME/T toxicity predictions, and DFT study of two trendy ortho vanillin-based scaffolds. *Heliyon* **2023**, *9*, No. e16057.
(14) (a) Majumdar, D. J.; Philip, J. E.; Dubey, A.; Tufail, A.; Roy, S. Synthesis, spectroscopic findings, SEM/EDX, DFT, and single-crystal structure of Hg/Pb/Cu−SCN complexes: *In silico* ADME/T profiling and promising antibacterial activities. *Heliyon* **2023**, *9*, No. e16103. (b) Guerroudj, A. R.; Boukabcha, N.; Benmohammed, A.; Dege, N.; Belkafouf, N. El. H; Khelloul, N.; Djafri, A.; Chouaih, A. Synthesis, crystal structure, vibrational spectral investigation, intermolecular interactions, chemical reactivity, NLO properties and molecular docking analysis on (E)-N-(4-nitrobenzylidene)-3-chlorobenzenamine: A combined experimental and theoretical study. *J. Mol. Struct.* **2021**, *1240*, No. 130589. (c) Ilmi, R.; Zhang, D.; Dutra, J. D. L; Dege, N.; Zhou, L.; Wong, W.-Y.; Raithby, P. R.; Khan, M. S. *Org. Electron.* **2021**, *96*, No. 106216. (d) Tamer, Ö; Mahmoody, H.; Feyzioğlu, K. F.; Kılınç, O.; Avci, D.; Orun, O.; Dege, N.; Atalay, Y. Synthesis of the first mixed ligand Mn (II) and Cd (II) complexes of 4-methoxy-pyridine-2-carboxylic acid, molecular docking studies and investigation of their anti-tumor effects *in vitro*. *Appl. Organomet. Chem.* **2020**, *34* (3), No. e5416.
(15) (a) Chavez-Urias, I. F.; Lopez-Gonzalez, L. E.; Plascencia-Martinez, D. F.; Garcia, J. J.; Flores-Alamo, M.; Sugich-Miranda, R.; Medrano, F.; Picos-Corrales, L. A.; Lopez-Gastelum, K.-A.; Velazquez-Contreras, E. F.; Rocha-Alonzo, F. l-Isoleucine-Schiff Base Copper(II) Coordination Polymers: Crystal Structure, Spectroscopic, Hirshfeld Surface, and DFT Analyses. *ACS Omega* **2023**, *8*, 24601−24614. (b) Yusuf, T. L.; Oladipo, S. D.; Zamisa, S.; Kumalo, H. M.; Lawal, I. A.; Lawal, M. M.; Mabuba, N. Design of New Schiff-Base Copper(II) Complexes: Synthesis, Crystal Structures, DFT Study, and Binding Potency toward Cytochrome P450 3A4. *ACS Omega* **2021**, *6*, 13704−13718. (c) Hussain, R.; Rubab, S. L.; Maryam, A.; Ashraf, T.; Arshad, M.; Lal, K.; Sumrra, S. H.; Ashraf, S.; Ali, B. Synthesis, Spectroscopic and Nonlinear Optical Properties, and Antimicrobial Activity of Cu(II), Co(II), and Ni(II) Complexes: Experimental and Theoretical Studies. *ACS Omega* **2023**, *8* (45),

https://doi.org/10.1021/acsomega.4c09312
ACS Omega 2025, 10, 14770−14786

42598−42609. (d) Avcı, D.; Altürk, S.; Sönmez, F.; Tamer, Ö; Başoğlu, A.; Atalay, Y.; Zengin Kurt, B.; Öztürk, D.; Dege, N. A new dinuclear copper (II) complex of 2,5−Furandicarboxyclic acid with 4(5)-Methylimidazole as a high potential α-glucosidase inhibitor: Synthesis, Crystal structure, Cytotoxicity study, and TD/DFT calculations. *Appl. Organomet. Chem.* **2019**, *33*, No. e4725.
(16) Shakir, M.; Hanif, S.; Sherwani, M. A.; Mohammad, O.; Al-Resayes, S. I. Pharmacologically significant complexes of Mn(II), Co(II), Ni(II), Cu(II) and Zn(II) of novel Schiff base ligand, (E)-N-(furan-2-yl methylene) quinolin-8-amine: Synthesis, spectral, XRD, SEM, antimicrobial, antioxidant and *in vitro* cytotoxic studies. *J. Mol. Struct.* **2015**, *1092*, 143−159.
(17) Ozturk, I.; Tunçel, A.; Yurt, F.; Biyiklioglu, Z.; Ince, M.; Ocakoglu, K. Antifungal photodynamic activities of phthalocyanine derivatives on *Candida albicans*. *Photodiagn. Photodyn. Ther.* **2020**, *30*, No. 101715.
(18) (a) Chakraborty, J.; Thakurta, S.; Samanta, B.; Ray, A.; Pilet, G.; Batten, S. R.; Jensen, P.; Mitra, S. Synthesis, characterisation and crystal structures of three trinuclear cadmium (II) complexes with multidentate Schiff base ligands. *Polyhedron* **2007**, *26*, 5139−5149. (b) SMART & SAINT *Software Reference manuals Version 6.45*; Bruker Analytical X-ray Systems, Inc.: Madison, WI, 2003. (c) *SHELXTL Reference Manual Ver. 6.1*; Bruker Analytical X-ray Systems, Inc.: Madison, WI, 2000. (d) Dolomanov, O. V.; Bourhis, L. J.; Gildea, R. J.; Howard, J. A. K; Puschmann, H. OLEX2: a complete structure solution, refinement and analysis program. *J. Appl. Crystallogr.* **2009**, *42*, 339−341. (e) Sheldrick, G. M. *Acta Crystallogr.* **2008**, *A64*, 112. (f) Sheldrick, G. M. *SHELXTL, a software for empirical absorption correction Ver.6.12*; Bruker AXS Inc.: WI. Madison, 2001.
(19) (a) Grimme, S. Semiempirical hybrid density functional with perturbative second-order correlation. *J. Chem. Phys.* **2006**, *124*, No. 034108. (b) Hay, P. J.; Wadt, W. R. Ab initio effective core potentials for molecular calculations. Potentials for the transition metal atoms Sc to Hg. *J. Chem. Phys.* **1985**, *82*, 270−283.
(20) Frisch, M. J.; Trucks, G. W.; Schlegel, H. B.; Scuseria, G. E.; Robb, M. A.; Cheeseman, J. R.; Scalmani, G.; Barone, V.; Petersson, G. A.; Nakatsuji, H.; Li, X.et al.*Gaussian 16*, Revision A. 03, Gaussian, Inc.: Wallingford CT, 3 2016.
(21) Roy, D. D.; Todd, A. K.; John, M. M. *Gauss View 5.0. 8*; Gaussian, Inc.: Wallingford, 2009.
(22) Chaudhary, T.; Chaudhary, M. K.; Jain, S.; Tandon, P.; Joshi, B. D. The experimental and theoretical spectroscopic elucidation of molecular structure, electronic properties, thermal analysis, biological evaluation, and molecular docking studies of isococculidine. *J. Mol. Liq.* **2023**, *391*, No. 123212.
(23) Mchiri, C.; Gassoumi, B.; Acherar, S.; El-Sharief, M. A. M. S.; Nasri, H. Synthesis, X-ray molecular structure and QTAIM and NCI-RDG theoretic studies of a new cadmium (II) (4′4 diaminodiphenylmethane) (meso-arylporphyrin) coordination compound. *Inorg. Chem. Commun.* **2021**, *133*, No. 108924.
(24) (a) Weigend, F. Accurate Coulomb-fitting basis sets for H to Rn. *Phys. Chem. Chem. Phys.* **2006**, *8*, 1057−1065. (b) Caldeweyher, E.; Bannwarth, C.; Grimme, S. Extension of the D3 dispersion coefficient model. *J. Chem. Phys.* **2017**, *147*, No. 034112. Frisch, M. J.; Trucks, G. W.; Schlegel, H. B.; Scuseria, G. E.; Robb, M. A.; Cheeseman, J. R.; Scalmani, G.; Barone, V.; Petersson, G. A.; Nakatsuji, H.; Li, X.; Caricato, M.; Marenich, A. V.; Bloino, J.; Janesko, B. G.; Gomperts, R.; Mennucci, B.; Hratchian, H. P.; Ortiz, J. V.; Izmaylov, A. F.; Sonnenberg, J. L.; Williams-Young, D.; Ding, F.; Lipparini, F.; Egidi, F.; Goings, J.; Peng, B.; Petrone, A.; Henderson, T.; Ranasinghe, D.; Zakrzewski, V. G.; Gao, J.; Rega, N.; Zheng, G.; Liang, W.; Hada, M.; Ehara, M.; Toyota, K.; Fukuda, R.; Hasegawa, J.; Ishida, M.; Nakajima, T.; Honda, Y.; Kitao, O.; Nakai, H.; Vreven, T.; Throssell, K.; Montgomery, J. A., Jr.; Peralta, J. E.; Ogliaro, F.; Bearpark, M. J.; Heyd, J. J; Brothers, E. N.; Kudin, K. N.; Staroverov, V. N.; Keith, T. A.; Kobayashi, R.; Normand, J.; Raghavachari, K.; Rendell, A. P.; Burant, J. C.; Iyengar, S. S.; Tomasi, J.; Cossi, M.; Millam, J. M.; Klene, M.; Adamo, C.; Cammi, R.; Ochterski, J. W.; Martin, R. L.; Morokuma, K.; Farkas, O.; Foresman, J. B.; Fox, D. J. *Gaussian 16*, Revision C.01, Gaussian, Inc.: Wallingford CT, 2016.
(25) Bader, R. F. W. A quantum theory of molecular structure and its applications. *Chem. Rev.* **1991**, *91*, 893−928.
(26) Contreras-Garcia, J.; Johnson, E. R.; Keinan, S.; Chaudret, R.; Piquemal, J.-P; Beratan, D. N.; Yang, W. NCIPLOT: A Program for Plotting Noncovalent Interaction Regions. *J. Chem. Theory Comput.* **2011**, *7*, 625−632.
(27) Todd, A.; Keith, T. K.; *Gristmill Software*; AIMAll: (Version 19.10.12), Overland Park KS, USA, 2019, (aim.tkgristmill.com).
(28) Mahmoudi, G.; Lawrence, S. E.; Cisterna, J.; Cárdenas, A.; Brito, I.; Frontera, A.; Safin, D. A. *New J. Chem.* **2020**, *44*, 21100−21107.
(29) (a) Pérez-Laguna, V.; Gilaberte, Y.; Millán-Lou, M. I.; Agut, M.; Nonell, S.; Rezusta, A.; Hamblin, M. R. A combination of photodynamic therapy and antimicrobial compounds to treat skin and mucosal infections: a systematic review. *Photochem. Photobiol. Sci.* **2019**, *18*, 1020−1029. (b) Okamoto, I.; Miyaji, H.; Miyata, S.; Shitomi, K.; Sugaya, T.; Ushijima, N.; Akasaka, T.; Enya, S.; Saita, S.; Kawasaki, H. Antibacterial and antibiofilm photodynamic activities of lysozyme-Au nanoclusters/rose bengal conjugates. *ACS Omega* **2021**, *6*, 9279−9290.
(30) Waglewska, E.; Maliszewska, I.; Bazylińska, U. Antimicrobial phyto-photodynamic activity inducing by polyphenol-supported Methylene Blue co-loaded into multifunctional bilosomes: Advanced hybrid nanoplatform in the skin infections treatment. *Journal of Photochemistry and Photobiology B: Biology* **2023**, *240*, No. 112650.
(31) (a) Wang, R.; Cao, Y.; Jia, D.; Liu, L.; Li, F. New approach to synthesize 8-hydroxyquinoline-based complexes with Zn^{2+} and their luminescent properties. *Opt. Mater.* **2013**, *36*, 232−237. (b) Wang, X. H.; Shao, M. W.; Liu, L. Photoconductivity of a bundle of Bis (8-hydroxyquinoline) cadmium nanoribbons. *J. Mater. Sci.: Mater. Electron.* **2011**, *22*, 120−123.
(32) Dutta, B.; Paul, S.; Halder, S. Explosive and pollutant nitroaromatic sensing through a Cd (II) based ladder shaped 1D coordination polymer. *Heliyon* **2023**, *9*, No. e13504.
(33) (a) Velusamy, P.; Babu, R. R.; Ramamurthi, K.; Elangovan, E.; Viegas, J.; Dahlem, M. S.; Arivanandhan, M. Characterization of spray pyrolytically deposited high mobility praseodymium doped CdO thin films. *Ceram. Int.* **2016**, *42*, 12675−12685. (b) Sakee, U.; Wanchanthuek, R. Catalytic activity of bimetallic Zn/TiO2 catalyst for degradation of herbicide paraquat: Synthesis and characterization. *Mater. Res. Express* **2017**, *4*, No. 115504. (c) Luo, J.; Niu, Q.; Jin, M.; Cao, Y.; Ye, L.; Du, R. Study on the effects of oxygen-containing functional groups on Hg0 adsorption in simulated flue gas by XAFS and XPS analysis. *Journal of Hazardous Materials* **2019**, *376*, 21−28. (d) Akbari, S. S.; Karadas, F. 3D-Cobalt-Dicyanamide-Derived 2D-Layered-$Co(OH)_2$-Based Catalyst for Light-Driven Hydrogen Evolution. *ACS Omega* **2024**, *9*, 8585−8593. (e) Liu, J.; Zou, Y.; Cruz, D.; Savateev, A.; Antonietti, M.; Vilé, G. Ligand−Metal Charge Transfer Induced via Adjustment of Textural Properties Controls the Performance of Single-Atom Catalysts during Photocatalytic Degradation. *ACS Appl. Mater. Interfaces* **2021**, *13*, 25858−25867. (f) Chang, J. K.; Lee, M. T.; Tsai, W. T.; Deng, M. J.; Sun, I. W. X-ray photoelectron spectroscopy and in situ X-ray absorption spectroscopy studies on reversible insertion/desertion of dicyanamide anions into/from manganese oxide in ionic liquid. *Chem. Mater.* **2009**, *21*, 2688−2695. (g) Hashimoto, H.; Ohno, A.; Nakajima, K.; Suzuki, M.; Tsuji, H.; Kimura, K. Surface characterization of imidazolium ionic liquids by high-resolution Rutherford backscattering spectroscopy and X-ray photoelectron spectroscopy. *Surf. Sci.* **2010**, *604*, 464−469. (h) Kruszynski, R.; Sierański, T. Can Stacking Interactions Exist Beyond the Commonly Accepted Limits? *Cryst. Growth Des.* **2016**, *16*, 587−595.
(34) (a) Dhifet, M.; Gassoumi, B.; Lutoshkin, M. A.; Kazachenko, A. S.; Kazachenko, A. S.; Al-Dossary, O.; Issaoui, N.; Nasri, H. Synthesis, X-ray Crystallography, Spectroscopic Characterizations, Density Functional Theory, and Hirshfeld Surface Analyses of a Novel (Carbonato) Picket Fence Iron(III) Complex. *Molecules* **2024**, *29*,

https://doi.org/10.1021/acsomega.4c09312
ACS Omega 2025, 10, 14770−14786

3722. (b) Mkacher, H.; Gassoumi, B.; Dardouri, N. E.; Nasri, S.; Loiseau, F.; Molton, F.; Roisnel, T.; Turowska-Tyrk, I.; Ghala, H.; Acherar, S.; Nasri, H. Photophysical, cyclic voltammetry, electron paramagnetic resonance, X-ray molecular structure, DFT calculations and molecular docking study of a new Mn(III) metalloporphyrin. *J. Mol. Struct.* **2025**, *1319*, No. 139455. (c) Benjamin, I.; Ekpong, B. O.; Abdullah, H. Y.; Agwamba, E. C.; Anyambula, I. A.; Adedapo, S. A.; Louis, H. Surface modification of transition metals (TM: Mn, Fe, Co) decorated Pt-doped carbon quantum dots (Pt@CQDs) nanostructure as nonenzymatic sensors for nitrotyrosine a biomarker for Alzheimer: Perspective from density functional theory. *Materials Science in Semiconductor Processing* **2024**, *174*, No. 108245. (d) Sooraj, M.; Manoj, E.; Prathapachandra Kurup, M. R. Solvothermal Self-Assembly of a Novel Metal-Organic Square Grid Complex Using a Biscarbohydrazone Ligand Building Block: Crystal Structures, Hirshfeld and Void Surface Analyses, Band Gap Calculations and DFT Studies. *Polyhedron* **2023**, *244*, No. 116583. (e) Srinivas, M.; Vijayakumar, G. R.; Mahadevan, K. M.; Nagabhushana, H.; Bhojya Naik, H. S. Synthesis, Photoluminescence and Forensic Applications of Blue Light Emitting Azomethine-Zinc (II) Complexes of Bis(Salicylidene)Cyclohexyl-1,2-Diamino Based Organic Ligands. *Journal of Science: Advanced Materials and Devices* **2017**, *2* (2), 156−164. (f) Abd-Elmageed, A. a. I.; Ibrahim, S. M.; Bourezgui, A.; Al-Hossainy, A. F. Synthesis, DFT Studies, Fabrication, and Optical Characterization of the [ZnCMC]TF Polymer (Organic/Inorganic) as an Optoelectronic Device. *New J. Chem.* **2020**, *44* (20), 8621−8637.

(35) (a) Hadi, H.; Bouzid, G.; Nasr, S.; Ghalla, H.; Chaabane, R. B.; Ayachi, S. Design, synthesis, and density functional theory studies of a new selective chemosensor for Pb2+. *Heliyon* **2023**, *9*, No. e20206. (b) Fasiuddin, G. S.; Basha, A. A.; Kubaib, A.; Azam, M.; Muzammil, P.; Bouzid, G.; Ayachi, S.; Khan, F. L. A; Imran, P. M.; Al-Resayes, S. I. Solvation model, Vibrational analysis, electronic level, non-covalent interactions and Molecular docking investigations of 6-Chloro-2-(4-Aminophenyl)-1H-Benzimidazole. *J. Mol. Liq.* **2024**, *398*, No. 124315. (c) Channar, P. A.; Saeed, A.; Larik, F. A.; Bolte, M.; Erben, M. F. Ibuprofen-Thiadiazole Hybrid Compounds: Synthesis, Vibrational Analysis and Molecular Structure of 5-(1-(4-Isobutylphenyl)Ethyl)-1,3,4-Thiadiazol-2-Amine Hydrochloride. *J. Mol. Struct.* **2019**, *1179*, 11−17.

(36) Espinosa, E.; Molins, E.; Lecomte, C. Hydrogen bond strengths revealed by topological analyses of experimentally observed electron densities. *Chem. Phys. Lett.* **1998**, *285*, 170−173.

(37) (a) Nashre-ul-Islam, S. M.; Dutta, D.; Frontera, A.; Bhattacharyya, M. K. Supramolecular association involving nitrile−nitrile interactions in polymeric Mn(II) coordination complexes: A combined experimental and theoretical study. *Inorg. Chim. Acta* **2019**, *487*, 424−432. (b) Dutta, D.; Sharma, P.; Frontera, A.; Gogoi, A.; Verma, A. K.; Dutta, D.; Sharma, B.; Bhattacharyya, M. K. Oxalato bridged coordination polymer of manganese(III) involving unconventional O···π-hole(nitrile) and antiparallel nitrile···nitrile contacts: antiproliferative evaluation and theoretical studies. *New J. Chem.* **2020**, *44*, 20021−20038. (c) Sarkar, R. S.; Basak, T.; Gomila, R. M.; Frontera, A.; Chattopadhyay, S. DFT study on CH···O, CH···SCN and S···π interaction energies in three dinuclear mixed valence cobalt(III/II) complexes with secondary diamine ligands having inner N_2O_2 and outer O_4 compartments. *Polyhedron* **2022**, *225*, No. 116039.

(38) (a) Abdelaziz, B.; Chérif, I.; Gassoumi, B.; Patanè, S.; Ayachi, S. Linear and Nonlinear Optical Responses of Nitrobenzofurazan-Sulfide Derivatives: DFT-QTAIM Investigation on Twisted Intramolecular Charge Transfer. *J. Phys. Chem. A* **2023**, *127*, 9895−9910. (b) Pritha, P.; Kishore, G.; Xavier, S.; Paularokiadoss, F.; Bhakiaraj, D.; Periandy, S.; Bouzid, G.; Ayachi, S. Sunlight-activated dye degradation of ZnO/CdO-decorated graphene oxide and its antibacterial activity. *Mater. Chem. Phys.* **2024**, *326*, No. 129829. (c) Hadi, H.; Chouchen, B.; Nasr, S.; Bouzid, G.; Chérif, I.; Basha, A.; Kubaib, A.; Imran, P. M.; Caccamo, M. T.; Ladhari, T.; Ayachi, S. Exploring high-performance functionalized corannulene dimers: A DFT-based investigation for novel photovoltaic applications. *Synth. Met.* **2024**, *302*, No. 117543.

(39) (a) Damena, T.; Alem, M. B.; Zeleke, D.; Desalegn, T.; Eswaramoorthy, R.; Demissie, T. B. Synthesis, characterization, and biological activities of zinc(II), copper(II) and nickel(II) complexes of an aminoquinoline derivative. *Front. Chem.* **2022**, *10*, No. 1053532. (b) Montaña, A. M.; Batalla, C. The Rational Design of Anticancer Platinum Complexes: The Importance of the Structure-Activity Relationship. *Curr. Med. Chem.* **2009**, *16*, 2235−2260. (c) Meléndez, C. M.; Barraza, G. A.; Sojo, F.; Arvelo, F.; Kouznetsov, V. V. Substituted 2-arylquinoline and 2-methyl-1,2,3,4- tetrahydroquinoline derivatives with selective anticancer activity: synthesis, structure−activity relationships, and molecular modelling insights. *New J. Chem.* **2024**, *48*, 19674−19690.

(40) Majumdar, D.; Philip, J. E.; Gassoumi, B.; Ayachi, S.; Abdelaziz, B.; Tüzün, B.; Roy, S. Supramolecular clumps of μ2−1,3-acetate bridges of Cd(II)-Salen complex: Synthesis, spectroscopic characterization, crystal structure, DFT quantization's, and antifungal photodynamic therapy. *Heliyon* **2024**, *10*, No. e29856.

https://doi.org/10.1021/acsomega.4c09312
ACS Omega 2025, 10, 14770−14786